Interactions between Gravity Waves and Cold Air Outflows in a Stably Stratified Uniform Flow

YUH-LANG LIN, TING-AN WANG, AND RONALD P. WEGLARZ

Department of Marine, Earth, and Atmospheric Sciences, North Carolina State University, Raleigh, North Carolina

(Manuscript received 1 September 1992, in final form 19 April 1993)

ABSTRACT

Interactions between gravity waves and cold air outflows in a stably stratified uniform flow forced by various combinations of prescribed heat sinks and sources are studied using a hydrostatic two-dimensional nonlinear numerical model. It is found that the formation time for the development of a stagnation point or reversed flow at the surface is not always directly proportional to the Froude number when wave reflections exist from upper levels. It is shown that a density current is able to form by the wave–outflow interaction, even though the Froude number is greater than a critical value. This is the result of the wave–outflow interaction shifting the flow response to a different location in the characteristic parameter space. A density current is able to form or be destroyed due to the wave–outflow interaction between a traveling gravity wave and a cold air outflow. This is proved by performing experiments with a steady-state heat sink and an additional transient heat source. In a quiescent fluid, a region of cold air, convergence, and upward motion is formed after the collision between two outflows produced by two prescribed heat sinks. After the collision, the individual cold air outflows lose their own identity and merge into a single, stationary, cold air outflow region. Gravity waves tend to suppress this new stationary cold air outflow after the collision. The region of upward motion associated with the collision is confined to a very shallow layer. In a moving airstream, a density current produced by a heat sink may be suppressed or enhanced nonlinearly by an adjacent heat sink due to the wave–outflow interaction.

1. Introduction

It has long been recognized that the evaporative cooling associated with the precipitation falling within the downdraft of a mesoscale convective cloud line or an isolated thunderstorm provides a quasi-stationary heat sink to the environmental flow (e.g., see Thorpe et al. 1980). This evaporative cooling tends to produce dense, diabatically cooled air that descends from above the cloud base to form cold outflows, which are able to propagate away from the convective line or the storm. This gravity-driven outflow is often called a density current. Simpson (1982) defined a density or gravity current as the flow of one fluid within another resulting from the density difference between the two fluids. Thus, the diabatically forced gravity-driven outflow accompanying mesoscale convective downdrafts may be called a density current. The passage of this density current on the surface is marked by a pressure jump or rapid rise, a rapid change in wind speed and direction, temperature, and relative humidity commonly associated with a propagating gust front. Ahead of the propagating density current, the air is forced to ascend and condensation may occur over the gust front (Seitter 1986). This lifting process has been considered to be responsible for triggering new convective cells. The new convective cell may either join the original long-lasting single convective cell (Ludlam 1963; Newton 1966) or become part of the convective system, which consists of many ordinary, short-lived cells in tropical squall lines (Zipser 1969). This mechanism is important in the generation and maintenance of severe long-lasting moist convection as found from observational work (e.g., Charba 1974; Goff 1975; Sinclair and Purdom 1983; Mueller and Carbone 1987) and simulated in recent numerical modeling work (e.g., Mitchell and Hovermale 1977; Thorpe et al. 1982; Droegemeier and Wilhelmson 1985a,b; Rotunno et al. 1988) on such systems. Therefore, it is essential to understand the formation of the density current associated with convective systems.

The formation of a density current is closely related to the response of a stably stratified flow to the evaporative cooling. The latter problem has been investigated mathematically by prescribing either the thermal forcing (e.g., Smith and Lin 1982; Lin and Smith 1986; Raymond 1986; Bretherton 1988) or the momentum forcing (Crook and Moncrieff 1988). However, in order to study the formation of the density current, nonlinear effects must be considered since the density current propagates against the basic wind. Recently, Raymond and Rotunno (1989, denoted as RR hereafter)

Corresponding author address: Dr. Yuh-Lang Lin, Department of Marine, Earth and Atmospheric Sciences, North Carolina State University, Box 8208, Raleigh, NC 27695-8208.

studied the response of a uniform stably stratified flow to prescribed cooling with emphasis on the formation of the density current. In their nonlinear numerical modeling study, RR defined four different regimes that are based on the two nondimensional parameters, $F = |U|/(Qdl)^{1/3}$ and $G = \pi|U|/Nd$, where U is the basic wind speed, Q the buoyancy depletion rate, d the depth of the cooling region, and l the width of the cooling region. The buoyancy depletion rate, in units of kelvins per second, defined by RR is equal to gQ_0/c_pT_0 in the present dimensional form used in this study, where Q_0 has the units of joules per kilogram per second. Thus, the definition of F becomes

$$F = |U|/[g|Q_0|dl/c_pT_0]^{1/3}.$$

The first nondimensional parameter (F) has been defined by Thorpe et al. (1980) in a numerical investigation of the nonlinear response of an unstratified flow to prescribed cooling. It is noteworthy to mention that the F and G parameters in RR are derived from a linear analysis. In contrast, Lin and Chun (1991) derived F and G parameters in the more general case in which the effects of vertical wind shear were quantitatively explored with the help of a fully nonlinear model. In addition, based on a number of numerical simulations and the idealized characteristic function, $F_c = F_0\{G^2/(G^2 + G_0^2)\}^{1/3}$, RR have determined the actual curve $F_c(G)$ in their F–G parameter space. Based on this curve and under the assumption that the critical value $G_c = 1$, flow responses are classified into four different regimes: (i) supercritical to both outflows and gravity waves ($F > F_c$ and $G > G_c$), (ii) supercritical to outflows and subcritical to gravity waves ($F > F_c$ and $G < G_c$), (iii) subcritical to both outflows and gravity waves ($F < F_c$ and $G < G_c$), and (iv) subcritical to outflows and supercritical to gravity waves ($F < F_c$ and $G > G_c$). These responses are illustrated in Fig. 1.

With the above classification, it is found that the dynamic behavior of the disturbance sometimes resembles a thermally forced gravity wave rather than a density current (RR). This type of behavior in the flow response field has also been simulated in numerical modeling studies investigating the dynamical effects of vertical wind shear in midlatitude squall line environments to prescribed thermal forcing (Lin and Chun 1991). The relevance of solitarylike gravity waves as an additional class of disturbances was discussed by Dudhia et al. (1987) and by Crook and Moncrieff (1988). The gravity wave speed also defines a minimum propagation speed for a self-regenerating convective system. Lin and Chun (1991) have extended the work of RR to a stably stratified shear flow with a critical level.

In the real atmosphere, waves generated in the layer near the surface may be reflected back since the fluid is often structured when latent heating and vertical wind shear exist. One example is that when $l_1^2 - l_2^2 > \pi^2/H^2$, where H is the height of the lower layer and l_1 and l_2 are the Scorer parameters of the lower and upper layers, respectively, lee waves tend to occur for flow over orography since the wave energy is trapped in the lower layer (Scorer 1949). This situation may also occur in the nocturnal boundary layer. Another example is the wave ducting mechanism proposed by Lindzen and Tung (1976). They showed that a stable wave duct adjacent to the surface becomes an efficient wave reflecting mechanism when it is capped by a dynamically unstable shear layer with a critical level. Although Lindzen and Tung considered a dry and otherwise simple atmosphere, a similar wave duct may also exist in the large-scale setting of a convective cloud line.

The interaction between the outflows produced by two adjacent thunderstorms may play a crucial role in triggering deep convection. One example is the interaction of two thunderstorms observed on 15 June 1973 in the Florida Area Cumulus Experiment (FACE) (Holle and Maier 1980). The interaction of two thunderstorm outflows in a moist shear flow has been investigated by Droegemeier and Wilhelmson (1985a,b) using a three-dimensional numerical cloud model. The wind shear vector was assumed to be perpendicular to the line containing the two initial outflow-producing clouds. They found that ambient air in the outflow collision region is literally "squeezed" out of the way as the two outflows collide. Some of this air is lifted to saturation, triggering convective clouds. It also has been found that the cumulus downdrafts and associated cold air outflows play a dominant role in the cloud merging process. That is, one or more new convective cells start to grow at a cloud bridge that is formed by the merging of two cold outflows associated with the downdrafts (Simpson 1980; reviewed by Westcott 1984). This mechanism has also been found in numerical simulations (Tao and Simpson 1984). In addition, Lin and Smith (1986) and Lin and Chun (1991) have shown that internal gravity waves can be triggered by the diabatic cooling. Schmidt and Cotton (1990) have also found that interactions exist between upper- and lower-level gravity waves in simulating midlatitude squall lines. However, the dynamical influence that gravity waves exert on the interaction between two density currents when wave reflection exists from above deserves a fundamental study under the hypothesis that these thermally forced gravity waves may then interact with the cold air outflows.

The objective of this study is to investigate the interactions between gravity waves and cold air outflows in a stably stratified uniform flow forced by prescribed heat sinks using a two-dimensional nonlinear model with wave reflections from model top present. The nonlinear hydrostatic numerical model used in this study will be described in section 2. The use of a hydrostatic system is justified since the overall balances that determine density current propagation are essentially hydrostatic, although the details of the motion near the head of a density current are nonhydrostatic

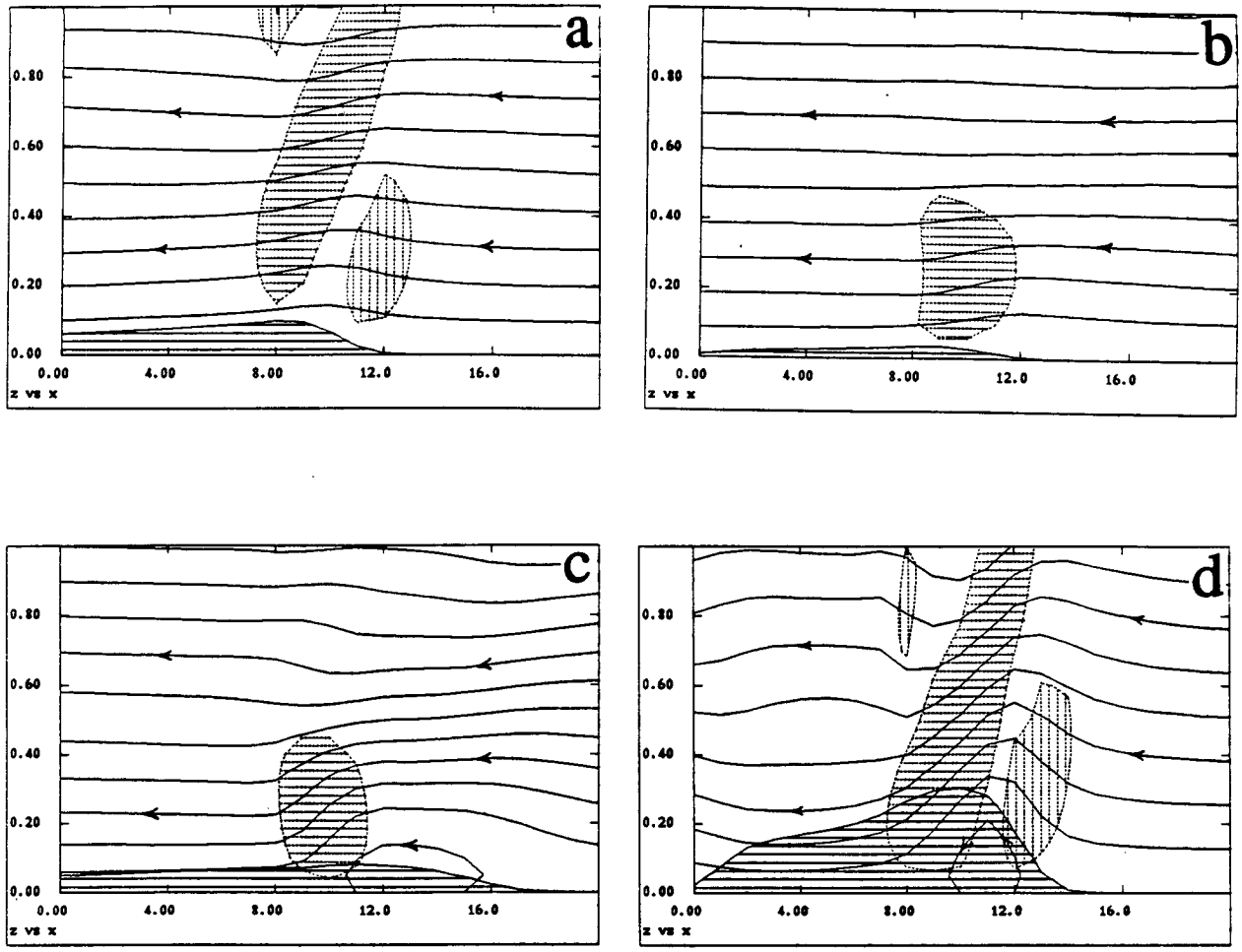

FIG. 1. Flow responses in different regimes proposed by RR: (a) supercritical relative to both waves and material outflow, (b) subcritical relative to waves and supercritical relative to material outflow, (c) subcritical relative to both waves and material outflows, and (d) supercritical relative to waves and subcritical relative to material outflow. Streamlines are shown by solid lines, while the dashed hatching shows regions of significant vertical motion. Vertical hatching indicates upward motion, while horizontal hatching indicates downward motion. Solid horizontal hatching shows the cold pool (after RR).

(RR). For the flow studied in this paper, the Scorer parameter (N/U) is much greater than the horizontal wavenumber $(k = 2\pi/l)$. This allows us to use the hydrostatic approximation as a first approach to the problem. In section 3, an anomaly in the formation of a reversed flow or a stagnation point at the surface due to the presence of reflected waves in the environment is presented and discussed. We will show that the critical curve F_c in the F–G parameter space is not always a simple smooth monotonic curve as found by RR, based on linear analysis when wave reflection exists from the upper levels. The effects of cooling-induced internal gravity waves on the formation of density currents will be investigated in section 4. The interaction between gravity waves and cold air outflows will be presented in section 5. Concluding remarks are given in the last section.

2. The model

In this study, we adopt a simple two-dimensional nonlinear numerical model that governs the evolution of thermally forced, finite amplitude perturbations excited within a hydrostatic, nonrotating, Boussinesq fluid. The zonal horizontal momentum equation, thermodynamic energy equation, incompressible continuity equation, and hydrostatic approximation to the vertical momentum equation may be written as

$$\frac{\partial u}{\partial t} + (U + u)\frac{\partial u}{\partial x} + w\left(\frac{\partial U}{\partial z} + \frac{\partial u}{\partial z}\right) = -\frac{\partial \phi}{\partial x} - \nu u, \tag{1}$$

$$\frac{\partial \theta}{\partial t} + (U + u)\frac{\partial \theta}{\partial x} + w\left(\frac{\partial \theta}{\partial z} + \frac{N^2\theta_0}{g}\right) = \frac{\theta_0}{c_p T_0} q - \nu\theta, \tag{2}$$

$$\frac{\partial u}{\partial x} + \frac{\partial w}{\partial z} = 0, \tag{3}$$

$$\frac{\partial \phi}{\partial z} = g\frac{\theta}{\theta_0}, \tag{4}$$

where

t time
x horizontal coordinate
z vertical coordinate
u perturbation horizontal wind speed
w perturbation vertical wind speed
θ perturbation potential temperature
ϕ perturbation kinematic pressure (p/ρ_0)
ν coefficients of Rayleigh friction and Newtonian cooling
ρ_0 constant reference density
T_0 constant reference temperature
θ_0 constant reference potential temperature
U basic horizontal wind speed
N Brunt–Väisälä frequency
g gravitational acceleration
c_p specific heat of air at constant pressure
q diabatic forcing.

The basic-state fields are assumed to be functions of the vertical coordinate z only, and may be viewed as being representative of the horizontally averaged synoptic-scale setting in which the mesoscale circulations governed by the numerical model take genesis and subsequently evolve. The perturbation quantities (u, w, p, and θ) representing disturbances in the zonal wind, vertical velocity, pressure, and potential temperature fields are dependent functions of the independent variables x, z, and t.

This coupled set of hydrothermodynamic field equations is discretized and solved numerically over a computational domain of horizontal grid interval Δx and vertical grid interval Δz by the method of finite differencing. Spatial derivatives in the horizontal are approximated by a fourth-order central differencing scheme, while spatial derivatives in the vertical are approximated by a second-order central differencing scheme. The temporal derivatives are approximated by the traditional leapfrog method. The spatial and temporal discretizations employed are similar to those incorporated in the Drexel Limited Area Mesoscale Prediction System (LAMPS) (Perkey 1976) and in the two-dimensional nonlinear model used by Lin and Chun (1991).

Viscous effects are modeled through the inclusion of Rayleigh friction and Newtonian cooling terms in the horizontal momentum and thermodynamic energy equations, respectively. In this study, the coefficients of Rayleigh friction and Newtonian cooling are specified to be zero. Nonlinear aliasing is removed by applying a weak five-point numerical smoother derived from the fourth-order diffusion equation and is applied at each time step throughout the numerical integration. Divergence of the solution due to the time splitting inherent in the leapfrog scheme is reduced through the incorporation of a three-point temporal filter (Asselin 1972). The upper and lower boundaries of the computational domain place constraints on the disturbance flow field such that either (i) the flow component normal to the boundaries vanishes identically, or (ii) the Sommerfeld radiation condition is obeyed. Under option (i), it is obvious that either flat, rigid lids bound the vertical flow domain, or that the flow is constrained to follow the contours of the low-level orography. The radiation condition is approximated either by inclusion of an artificial sponge layer (Klemp and Lilly 1978) or the numerical algorithm proposed by Klemp and Durran (1983). Notice that with radiation conditions applied at both the upper and lower boundaries, disturbances in a continuously stratified, unbounded, hydrostatic, nonrotating Boussinesq flow may be investigated with this model. Wave reflection from the lateral boundaries is minimized by invoking radiation conditions that are approximated by numerical techniques originally proposed by Orlanski (1976). Earlier versions of this model have been generalized by Chun (1991) to explicitly include moist thermodynamics and the parameterization of subgrid-scale mixing processes. The numerical techniques may be summarized as follows:

(a) fourth-order finite-difference scheme in the horizontal
(b) second-order finite-difference scheme in the vertical
(c) leapfrog scheme in time
(d) three options for the upper and lower boundary conditions: radiation condition, sponge layer, and rigid lid
(e) open lateral boundary conditions
(f) free-slip condition at the lower boundary
(g) prescribed and parameterized thermal forcings, or explicit moisture budget
(h) five-point numerical smoothing in both the horizontal and vertical
(i) three-point numerical smoothing in time.

The prognostic equations, Eqs. (1) and (2), with values for every variable from two previous time steps are solved first to obtain u and θ. Then w and ϕ are calculated by the diagnostic equations, Eqs. (3) and (4). The x and z grid intervals are taken to be $\Delta x = 3$ km and $\Delta z = 150$ m, respectively. There are 64 grid points in x and 41 in z. The time interval Δt is 10 s. An unstaggered grid structure is adopted, which implies that the horizontal velocity is defined at the lower surface. This model has been rigorously tested against the

well-accepted linear theories of orographically and thermally forced stratified flows that are well documented in the literature, and used in a number of theoretically oriented studies (e.g., Lin and Chun 1991).

3. The anomaly in the formation of reversed surface flow

Since we are interested in studying the dynamical mechanisms responsible for the formation of reversed flow when a stably stratified uniform flow passes a region of prescribed cooling, our first objective is to obtain the time when the incoming flow reverses its direction at the surface. As mentioned in the Introduction, the formation of this reversed flow is essential for the formation of a density current. The cooling region is set at the center of the domain with a width of 18 km (l) and extends to a height of 3 km (d) above the surface. Unlike the cooling function used in RR, we add regions of weak compensative heating uniformly on both the upstream and downstream sides of the cooling region such that the net diabatic forcing is equal to zero at each vertical level. The addition of the compensative heating is adopted to avoid the problem of net cooling and yields a well-posed mathematical problem (Smith and Lin 1982; Lin and Smith 1986; Bretherton 1988). The cooling rate is a maximum at the center of the cooling region. The effect of the weak and widespread compensative heating on the flow is negligible (Smith and Lin 1982) and thus does not complicate the F and G functions. The zonal wind $U(z)$ is specified to be vertically homogeneous [i.e., constant with height, $U(z) = U$, $0 \leq z \leq z_T$] and is directed from right to left. The formation time of the reversed surface flow is assumed to be the instant when zero total x-direction wind speed exists at the surface (i.e., $U + u = 0$). The time limit imposed in the numerical simulations for the attainment of reversed flow at the surface is either 10 000 s or 36 000 s, that is, 2.78 or 10.0 h, respectively.

Figure 2a shows the time for the formation of a reversed surface flow or stagnation point at different Froude numbers when a rigid lid is placed at $z_T = 6$ km. The rigid lid provides a simple way to represent the wave reflection from the middle level of the troposphere, which may occur in a real, structured atmosphere. A large number of numerical experiments (570) were performed in the construction of this figure. The Froude number is defined as $\mathrm{Fr} = |U|/Nd$. The Froude number of concern here is associated with the environment, unlike the definitions commonly used in other studies of density currents, which define the Froude number associated with the density current (e.g., Droegemeier and Wilhelmson 1985a). Since N and d (the depth of the cooling region) are assumed to be constant ($N = 0.01\ \mathrm{s}^{-1}$ and $d = 3$ km) in this study, the Froude number is a function of U only. The basic wind velocity varies from -1 to $-30\ \mathrm{m\ s}^{-1}$ with an increment of $-1\ \mathrm{m\ s}^{-1}$, which corresponds to the Froude number ranging from 0.033 to 1. Each curve in the figure represents a certain cooling rate (Q_0) that ranges from -0.1 to $-1.0\ \mathrm{J\ kg}^{-1}\ \mathrm{s}^{-1}$ and from -2 to $-10\ \mathrm{J\ kg}^{-1}\ \mathrm{s}^{-1}$ with an increment of $-1\ \mathrm{J\ kg}^{-1}\ \mathrm{s}^{-1}$. The prescribed cooling is a simple way to represent the quasi-stationary evaporative cooling associated with falling precipitation. A cooling rate of $Q_0 = -1\ \mathrm{J\ kg}^{-1}\ \mathrm{s}^{-1}$ corresponds to a precipitation rate of 3.5 mm h^{-1}. This precipitation rate is calculated according to the formula used in Lin (1986), $Q_0 = \pi LR\rho_w/[2\rho_a(z_2 - z_1)]$, with $L = 2.5 \times 10^6\ \mathrm{J\ kg}^{-1}$, $\rho_w = 10^3\ \mathrm{kg\ m}^{-3}$, $\rho_a = 1.275\ \mathrm{kg\ m}^{-3}$, $z_2 = 3$ km, and $z_1 = 0$ km.

The first curve (leftmost) in Fig. 2a shows different cases with a cooling rate $Q_0 = -0.1\ \mathrm{J\ kg}^{-1}\ \mathrm{s}^{-1}$. The time for forming a reversed surface flow (for simplicity denoted as Tr) increases rapidly as Fr increases, as expected. No reversed flow forms within 10 h for $\mathrm{Fr} > 0.13$ since the cooling is relatively weak. For a cooling rate of $Q_0 = -0.3\ \mathrm{J\ kg}^{-1}\ \mathrm{s}^{-1}$, the flow response is similar to that for a cooling rate of $Q_0 = -0.1\ \mathrm{J\ kg}^{-1}\ \mathrm{s}^{-1}$ when Fr is less than 0.3. No reversed flow forms within 10 h when $0.3 < \mathrm{Fr} < 0.33$ for this particular forcing. However, for this cooling rate, it is interesting to note that a reversed surface flow is able to form within 10 h when $0.33 < \mathrm{Fr} < 0.43$. Within this range, the formation time of the stagnation point does not increase for an increase in the Froude number (i.e., Tr is not directly proportional to Fr within this range). This peculiar behavior of the flow response to stationary cooling has an important impact on the formation of the density current and will be described later.

Similar behavior of the flow response occurs under a cooling rate of $Q_0 = -0.4\ \mathrm{J\ kg}^{-1}\ \mathrm{s}^{-1}$, as shown in Fig. 2a. The turning point, wherein it takes less time to form a reversed flow or stagnation point as Fr increases, appears to occur at Fr = 0.33. This corresponds to a basic wind speed of 10 m s^{-1}. The cause of this turning point will be explained in the next paragraph. Curves representing cooling rates of $Q_0 = -0.7$ to $-4\ \mathrm{J\ kg}^{-1}\ \mathrm{s}^{-1}$ indicate that the flow response for these various forcings behave more or less like the flow response to a cooling rate of $Q_0 = -0.6\ \mathrm{J\ kg}^{-1}\ \mathrm{s}^{-1}$. That is, it takes a longer time to form a stagnation point when the Froude number increases. There exists some critical Fr below which little effect on the time of flow reversal is seen for increasing Fr, but above which further increases of Fr quickly prevent flow reversal. Besides, no turning points exist within 10 h since the time limitation is set to 10 h in these simulations. Compared with other curves, we may predict that it is possible to find some turning points in these curves if we increase the time limit of the simulations. Of course, it becomes physically unrealistic if one looks for a solution longer than 10 h since most long-lasting mesoscale convective systems rarely force any one particular point of the local environment for this period of time. The curve representative of $Q_0 = -5\ \mathrm{J\ kg}^{-1}\ \mathrm{s}^{-1}$ has a turning point at about Fr = 0.87, while the curves representing cool-

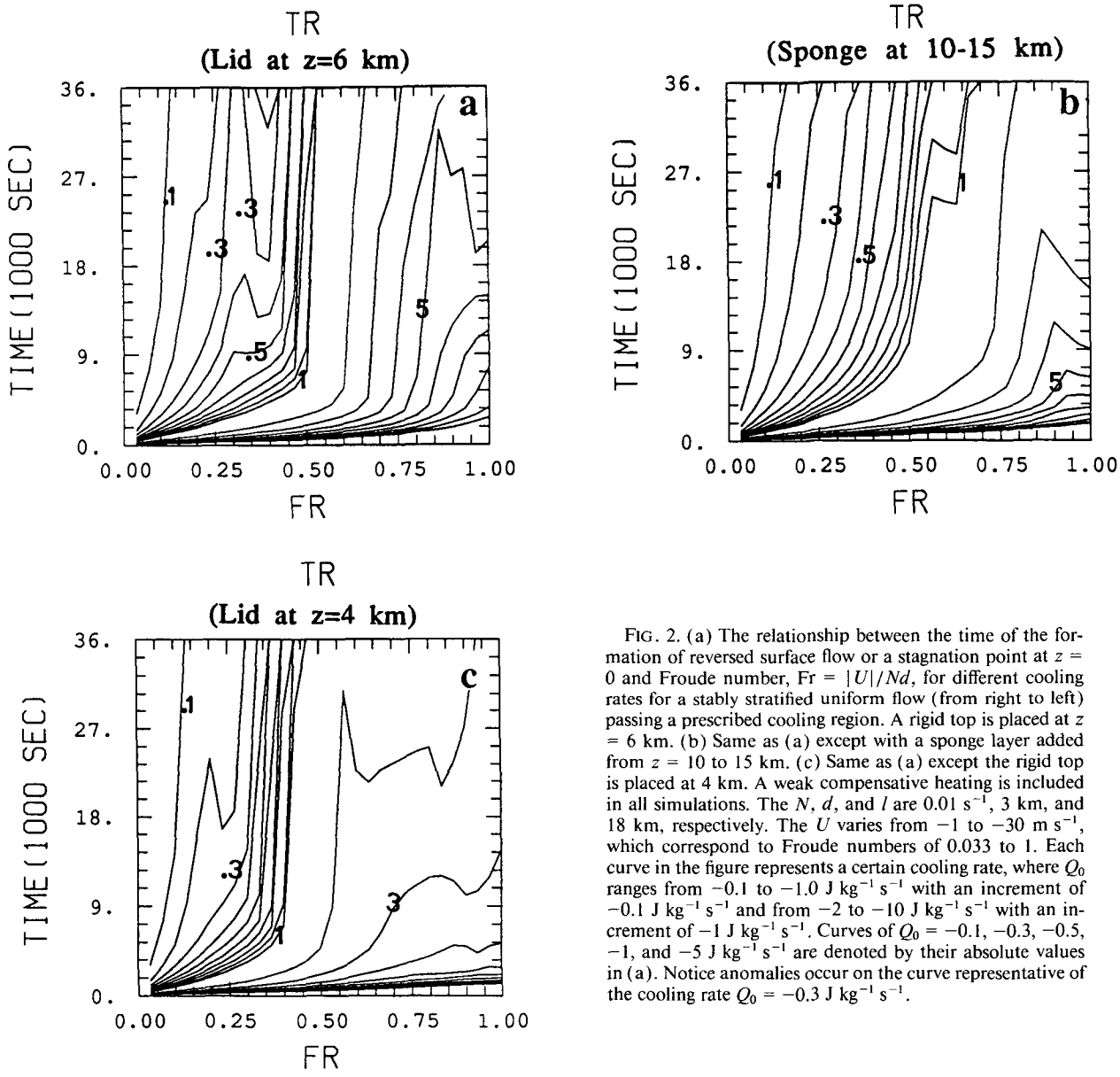

FIG. 2. (a) The relationship between the time of the formation of reversed surface flow or a stagnation point at $z = 0$ and Froude number, $\mathrm{Fr} = |U|/Nd$, for different cooling rates for a stably stratified uniform flow (from right to left) passing a prescribed cooling region. A rigid top is placed at $z = 6$ km. (b) Same as (a) except with a sponge layer added from $z = 10$ to 15 km. (c) Same as (a) except the rigid top is placed at 4 km. A weak compensative heating is included in all simulations. The N, d, and l are 0.01 s^{-1}, 3 km, and 18 km, respectively. The U varies from -1 to -30 m s^{-1}, which correspond to Froude numbers of 0.033 to 1. Each curve in the figure represents a certain cooling rate, where Q_0 ranges from -0.1 to -1.0 J kg^{-1} s^{-1} with an increment of -0.1 J kg^{-1} s^{-1} and from -2 to -10 J kg^{-1} s^{-1} with an increment of -1 J kg^{-1} s^{-1}. Curves of $Q_0 = -0.1$, -0.3, -0.5, -1, and -5 J kg^{-1} s^{-1} are denoted by their absolute values in (a). Notice anomalies occur on the curve representative of the cooling rate $Q_0 = -0.3$ J kg^{-1} s^{-1}.

ing rates of $Q_0 = -6$ and -7 J kg^{-1} s^{-1} have turning points at Fr = 1. The Tr for the curve representing $Q_0 = -10$ J kg^{-1} s^{-1} is about 2700 s for Fr = 1. It takes much less time to form a stagnation point in this case compared to the other cases since the cooling rate is much stronger.

In summary, Tr is shorter for a larger cooling rate than that for a smaller one for a fixed Froude number. If we fix the cooling rate and function, Tr does not always increase as the Froude number or the basic wind speed increases when wave reflections exist from upper levels. Figure 2b is similar to Fig. 2a except that a sponge layer exists in the layer between $z = 10$ km and $z = 15$ km. The prescribed cooling function here is chosen to be the same as that of RR. However, weak compensative heating is added. The behavior of the flow response, as indicated by the curves in Fig. 2b, is similar to Fig. 2a except no anomaly exists in the regime of small Froude number (i.e., highly nonlinear) flows. When a mechanism is provided such that the wave may be reflected back from a different level, this type of anomaly in the formation of a reversed surface flow or stagnation point may occur, too. One example is the second curve from the left representing the flow response to a prescribed cooling rate of $Q_0 = -0.2$ J kg^{-1} s^{-1} in Fig. 2c in which the rigid lid is placed at $z = 4$ km.

Figure 3 shows four F–G parameter maps for the numerical integration time limits of 10 000 s and 36 000 s. Each experiment is indicated by a symbol on

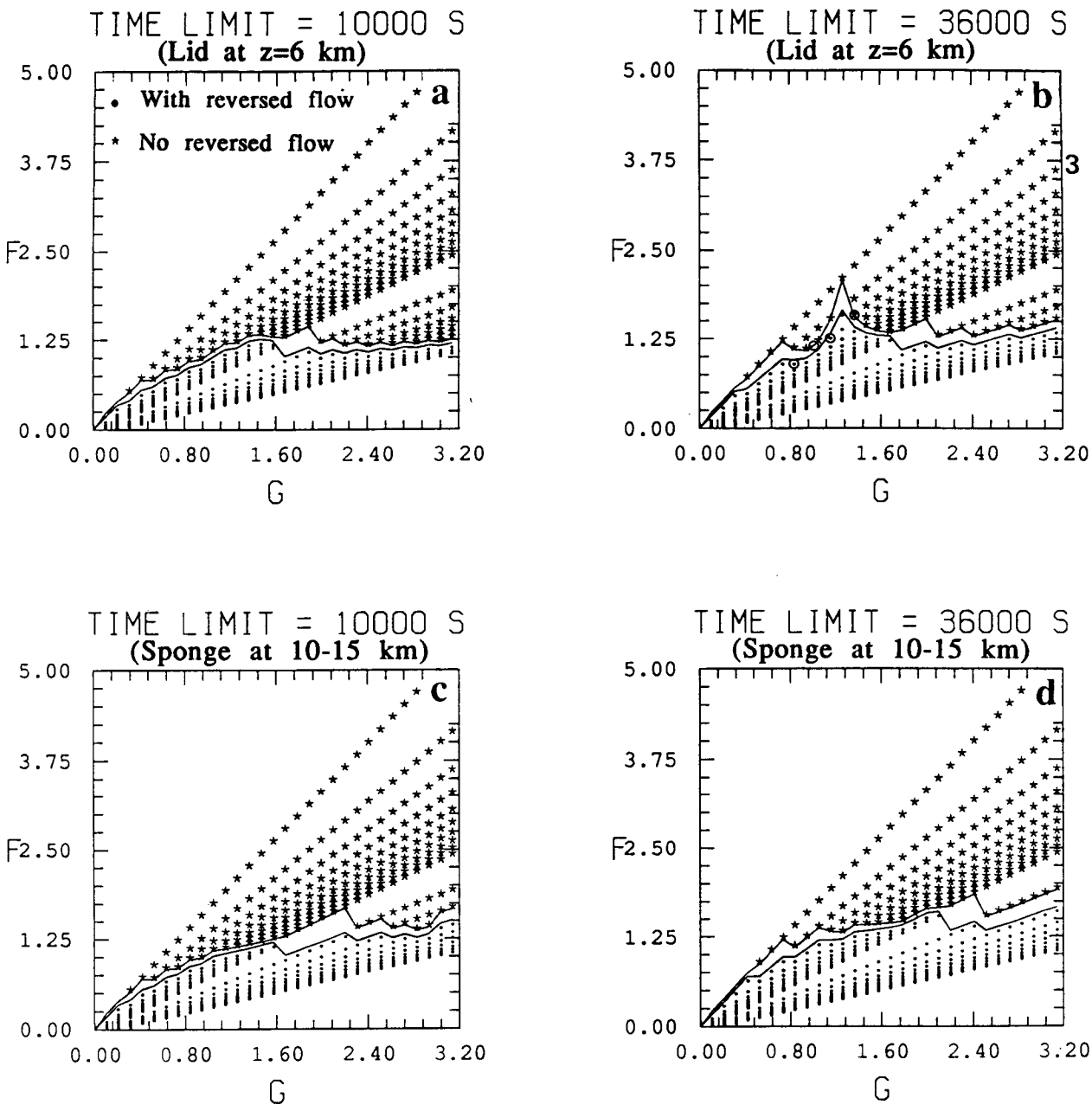

FIG. 3. (a) Based on Fig. 2a, a case is indicated with a dot on the F–G parameter map if the reversed surface flow or stagnation point forms before 10 000 s, and with an asterisk if it does not. (b) Same as (a) except for 36 000 s. (c) Same as (a) except with a sponge layer added from z = 10 to 15 km, and (d) same as (c) except for 36 000 s. Cases C1 to C4 are denoted by circles from left to right on curve 3 in (b). Notice the anomaly on curve 3. The parameters G and F are defined in Table 1.

the map. If a reversed surface flow exists before the end of the prescribed time limit, we indicate the case with a dot; if not, then with an asterisk. We draw two curves to separate the experiments into two groups, with and without reversed flow within the prescribed time limit. The upper curve connects the points with the greatest cooling rate among the simulated cases *that do not exhibit* the formation of a reversed surface flow for each corresponding G. The lower curve connects those cases that have the smallest cooling rate among the cases *that do exhibit* the formation of a reversed flow for each corresponding G. The actual critical curve is located in between these two curves. In RR, the time integration limit is taken to be 10 000 s. Since N and d are constant, the parameter G is proportional to $|U|$ only. In order to find the actual critical curve of the F–G map, we have performed a large number of numerical experiments.

Figure 3a shows the critical curves on the F–G parameter map for the time limit of 10 000 s.The critical curve is smooth and F_c increases monotonically to a value of about 1.25 as G increases from 0 to 1.6 (Fig. 3a), but it then remains about the same for any G greater than 1.6. If one chooses a time limit of 4000 s, then the critical curve will be smooth and monotonic as the idealized function proposed by RR based on linear analysis. The time limit chosen in Fig. 3b is 36 000 s. Here F_c increases almost linearly as G increases from 0 to 0.7. It becomes a concave curve in the range $0.7 < G < 1.28$. The curve then falls again until G equals 1.76 and then rises gradually for any G greater than this value. As shown in Fig. 3, one can always find a critical cooling rate for every basic wind speed (or equivalently G, because $G = \pi|U|/Nd$ and π/Nd is kept constant). For a fixed value of G and $F < F_c$, a stagnation point or reversed surface flow exists. This indicates that if the cooling rate is larger than the critical cooling rate for a fixed basic wind speed (constant G), then the flow response exhibits the existence of a stagnation point. Unlike that in RR, the critical curve (F_c) for a time limit of 36 000 s is neither smooth nor monotonic with G when wave reflections exist from above. Notice that the simulations for a fixed Q_0, N, d, and l are colinear with a slope of $Nd/(g|Q_0|\,dl/c_pT_0)^{1/3}$. This indicates that the flow response may change regimes from subcritical to supercritical, then back to subcritical flow again with respect to outflows as the basic wind speed increases. One example is the third curve (labeled as 3) from the upper right corner in Fig. 3b, which represents a cooling rate of $Q_0 = -0.3$ J kg^{-1} s^{-1}. Notice that this curve corresponds to the intersection of the third curve and the horizontal line at t = 36 000 in Fig. 2a since G is equal to πFr. This type of anomaly is also evident at an earlier time for a larger cooling rate such as the curve representing a cooling rate of $Q_0 = -0.4$ J kg^{-1} s^{-1} in Fig. 2a. We choose to make simulations based on curve 3 and a time limit of 10 h because it is easier to elucidate the interaction of gravity waves and outflows for a longer time. If one looks at the short time behavior, that is, $t \leq$ 36 000 s, then this anomalous flow response evidently does not occur.

As mentioned in the Introduction, RR have determined the actual curve $F_c(G)$ in their F–G parameter map, based on numerical simulations and the idealized characteristic function, $F_c = F_0\{G^2/(G^2 + G_0^2)\}^{1/3}$. We have repeated their calculations and find the actual curve for the case when the time limit of the numerical simulations is 10 000 s. Based on this analysis, some minor errors in the published values have been observed in the calculations of F in their Table 1, which yield a slightly different curve of $F_c(G)$ than is indicated by their Fig. 4. If we use these corrected values of F from those listed in their Table 1, the G_0 in their Eq. (11) will have a value of 2.6, instead of 1.65, in order to give the critical function $F_c(G)$. However, the general pattern of their idealized curves are very similar to the curves presented in Figs. 3c and 3d, and the minor discrepancy between the originally published values and the corrected values does not affect the general conclusions offered in that paper.

4. Effects of gravity waves on the formation of the density current

In order to study the mechanism associated with the abnormal behavior of the critical curve and its dynamical influence upon the formation of reversed flow or a stagnation point at the surface when wave reflection from aloft occurs, we have performed a number of numerical experiments with a fixed cooling rate of $Q_0 = -0.3$ J kg^{-1} s^{-1} and the rigid-lid condition imposed at the model top. These cases correspond to curve 3 (a straight line) in Fig. 3b. This curve intersects the critical curve (F_c) three times, since F_c is not monotonic with increasing G or $|U|$ when both N and d are fixed. The numerical experiments performed in this section are forced by cooling only. They are summarized in Table 1 and denoted by circles on curve 3 in Fig. 3b.

Figure 4 (C1) shows the time evolution of the response of a stably stratified, uniform flow over a region of stationary cooling of physical dimensions l = 18 km and d = 3 km. As mentioned earlier, compensative heating is added to avoid the net cooling problem. The basic wind velocity and cooling rate are -8 m s^{-1} and -0.3 J kg^{-1} s^{-1}, respectively. Notice that the basic wind blows from right to left. The time evolution of the total horizontal wind velocity at $z = 0$ is shown in Fig. 4a. The nondimensional flow parameters G and F are 0.84 and 0.96, respectively. The reversed surface flow forms at about t = 4 h as can be seen from the area of positive total wind velocity increasing smoothly with time at any instant thereafter. The region of maximum horizontal wind velocity then propagates to the upstream (right) side of the cooling region, although the temperature gradient along the cold air outflow at this time

TABLE 1. Summary of numerical experiments with one heat sink.

	Case			
	C1	C2	C3	C4
	Figure			
	4	5	6	7
U (ms^{-1})	−8	−9.5	−11	−13
Q_0 (J kg^{-1} s^{-1})	−0.3	−0.3	−0.3	−0.3
l (km)	18	18	18	18
d (km)	3	3	3	3
N (s^{-1})	0.01	0.01	0.01	0.01
Fr	0.27	0.32	0.37	0.43
G	0.84	1.00	1.15	1.36
F	0.96	1.14	1.32	1.56

* Fr = $|U|/Nd$, $G = \pi|U|/Nd$, $F = |U|/[g|Q_0|dl/c_pT_0]^{1/3}$

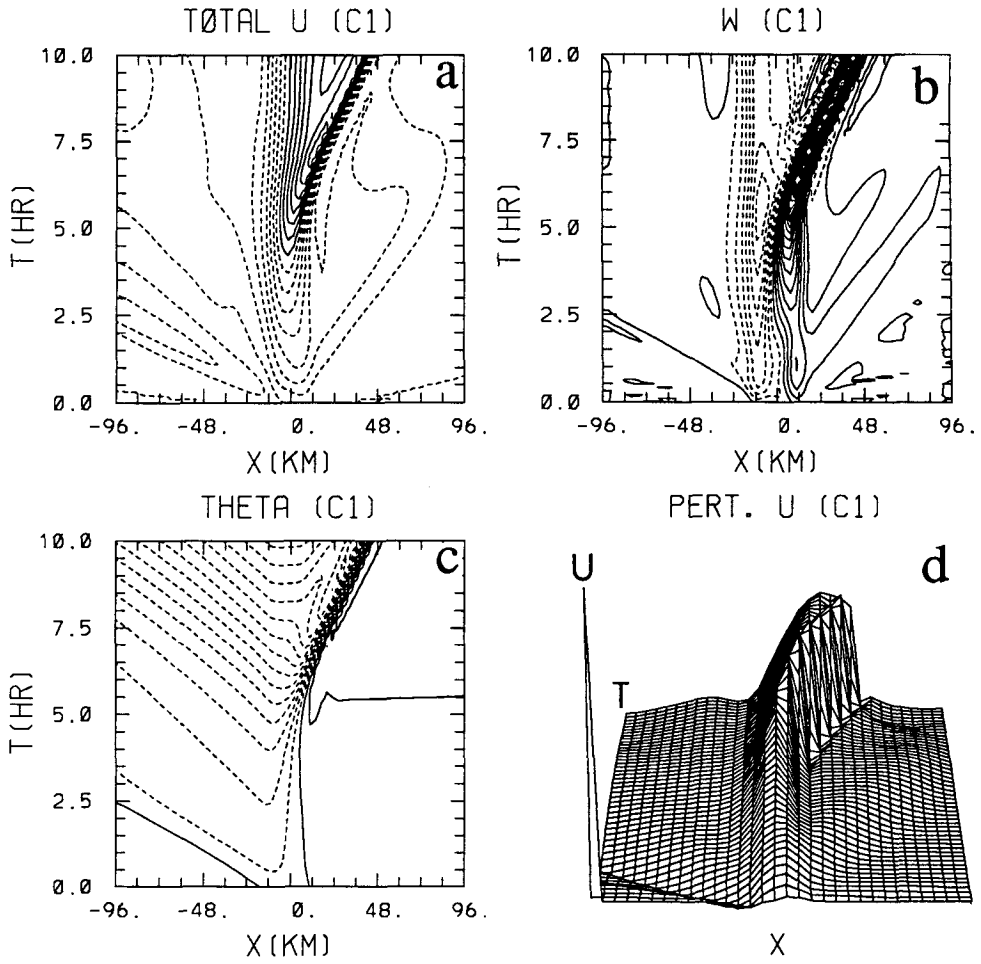

FIG. 4. (C1) Time evolution of the response for a stably stratified uniform flow passing over stationary cooling (l = 18 km, d = 3 km). The basic wind velocity and cooling rate are -8 m s^{-1} and -0.3 J kg^{-1} s^{-1}. Other flow parameters are listed in Table 1. Four fields of time evolution are shown: (a) total horizontal wind velocity ($U + u$) at $z = 0$, (b) w at $z = 150$ m, (c) θ at $z = 0$, and (d) 3D plot of u at $z = 0$. The

is still not sharp (Fig. 4c). The distinction between a cold air outflow and a density current seems rather arbitrary. Crook and Moncrieff (1988) identify a difference between density currents and solitary gravity waves in terms of reattachment of the dividing streamline passing the stagnation point. That is, a solitary gravity wave can exhibit a reversed flow but the stagnation streamline can reattach (Dudhia et al. 1987). On the other hand, Lin and Chun (1991) defined a density current as a cold air outflow propagating against the basic wind. This density current is also evident from the vertical wind field (Fig. 4b), the perturbation potential temperature field (Fig. 4c), and the perturbation horizontal wind field (Fig. 4d). The propagation speed of this density current is estimated to be about 2 m s^{-1}. For a flow with the same cooling rate, Brunt–Väisälä frequency, cooling depth, and whose basic wind speed is less than 8 m s^{-1}, a density current is able to form within 10 h since the pool of cold, dense air produced by the cooling has enough momentum to push against the relatively weak basic flow. This is also depicted in Fig. 3b. The frontal speed can be estimated from the response in a quiescent fluid (not shown) and is found to be about 5.3 m s^{-1}. The criterion for the formation of the density current is not simply determined by the relative magnitudes of the outflow speed, which is linearly proportional to $(g|Q_0|\,dl/c_pT_0)^{1/3}$, and the basic wind speed since the flow is highly nonlinear. In an unstratified flow, Thorpe et al. (1980) found that F_c is approximately equal to 1.4. It is also evident from Fig. 4a that two weak cooling-induced gravity waves exist, propagating in both the upstream and downstream directions. The upstream-propagating wave has a slower speed than the downstream wave since it propagates against the basic wind.

Figure 4b shows the time evolution of the vertical wind velocity at $z = 150$ m. Before the stagnation point forms at about $t = 4$ h, upward motion exists on the upstream side and downward motion on the downstream side of the cooling region. As time proceeds,

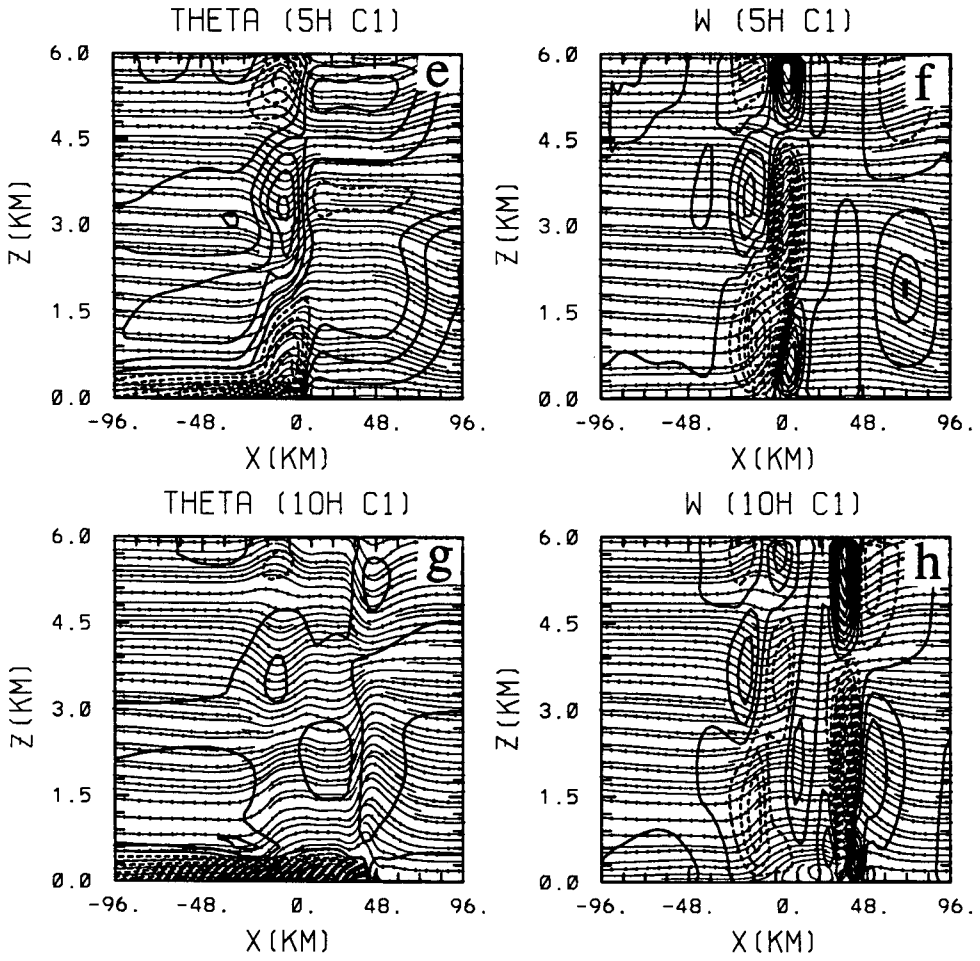

FIG. 4. (*Continued*) vertical structures with streamlines superimposed are shown in (e) θ at 5 h, (f) w at 5 h, (g) θ at 10 h, and (h) w at 10 h. The flow is subcritical to both outflows and gravity waves. The propagating wave mode, wave I, is denoted by I in (f). The contour intervals for (a), (b), (c), (e), (f), (g), and (h) are 1 m s^{-1}, 0.01 m s^{-1}, 0.6 K, 0.2 K, 0.04 m s^{-1}, 0.6 K, and 0.05 m s^{-1}, respectively.

the region of upward motion splits from the region of downward motion and propagates upstream. This split is associated with the development of the density current. Since the vertical velocity field shown in the figure is close to the surface, it is proportional to the low-level convergence field. Figure 4b also indicates that the density current is associated with the extremely strong convergence. Figure 4c shows the time evolution of the perturbation potential temperature field at the surface. The relatively cold area spreads far downstream of the cooling region as time proceeds. A very strong temperature gradient develops along the cold pool, which is much stronger than that associated with the cold air outflow in a weaker basic flow (Lin and Chun 1991). Figure 4d shows a three-dimensional plot of the time evolution of perturbation horizontal wind velocity at the surface. This plot provides a convenient way to view the time evolution of the associated subsequent wave structure and propagation. The scale at the origin is the amplitude of the perturbation horizontal velocity, which is plotted for comparison of wave magnitudes for different cases. In Fig. 4d, the strongest wave is located at the head of the density current. It can be seen that a weak gravity wave does propagate upstream, while another one propagates downstream. These two cooling-induced gravity waves correspond to those shown in Figs. 4a and 4b.

The vertical structure of the flow response at $t = 5$ h and $t = 10$ h for the present case (C1) is shown in Figs. 4e–h. The superimposed θ and streamline fields are shown in (e) and (g), while the vertical velocity and streamline fields are shown in (f) and (h). From Fig. 4a, the stagnation point or reversed flow is just beginning to form at about $t = 4$ h. The temperature gradient at the head of the density current ($x = 9.6$ km) at $t = 5$ h is sharper than that at earlier times (Fig. 4e). Both the potential temperature field and the vertical velocity field indicate that the flow structure has

a vertical wavelength of about 6 km, which is roughly 2 d as mentioned in RR. Near the surface, a portion of the cold air produced by the stationary cooling is advected downstream in a very shallow layer with a depth of about 1 km. It is interesting to note that not all of the prescribed cooling region ($0 < z < 3$ km) is occupied by the cold air. The upper portion of the prescribed cooling region ($2 \text{ km} < z$) is overcome by the adiabatic warming produced by the descending air. The effective cooling is reduced by this warm air. The structure of the vertical velocity field (Fig. 4f) exhibits the same vertical wavelength as evidenced in the perturbation potential temperature field. A region of strong upward motion with a maximum speed of about 0.16 m s^{-1} is produced near the head of the upstream cold air outflow, which is due to the convergence generated by the basic wind and the cold air outflow. On the downstream side of the prescribed cooling region, there exists downward motion. A counterclockwise rotor forms near the surface at the center of the cooling region, which is associated with the density current. The phase of the vertical velocity at $z = 3.6$ km is just opposite to that in the lower layer. This disturbance may be regarded as the thermally forced *stationary mode* of the gravity waves generated by the cooling. On the far upstream side at $x = 72$ km, a weak disturbance exists that is associated with an upstream-propagating wave. This wave may be regarded as the *propagating mode* of the thermally forced gravity waves generated by the prescribed cooling and is defined hereafter as wave I. It exhibits a larger vertical wavelength of roughly 8 km. Therefore, this case may be classified as *subcritical to both outflows and gravity waves* since both the outflow and gravity wave are able to propagate freely upstream.

At $t = 10$ h, the density current is well developed and has propagated upstream a distance of $x = 45$ km (Fig. 4g). Unlike the potential temperature field at $t = 5$ h, the cold air associated with the density current is wholly confined in a very shallow layer with a depth of about 1 km. This is because the cold air produced by the cooling is able to descend to the lower layer and propagate to both the upstream and downstream sides. Compared with this cold region, the temperature perturbation in the upper layer is very weak. The vertical velocity field (Fig. 4h) depicts two physically distinct waves. The stationary gravity wave mode near the cooling center, with a vertical wavelength of 6 km, is produced by the prescribed cooling, while the forced gravity wave near the density current, with a larger vertical wavelength, is produced by the density current. These two wave modes have also been found in a shear flow case as studied by Lin and Chun (1991). The gravity wave associated with the density current is much stronger than that associated with the cooling region since the low-level convergence near the density current is much stronger. The gravity wave forced by the density current should not be confused with the propagating wave mode (wave I) discussed earlier and in RR. At $t = 10$ h, wave I has already propagated beyond the right boundary of the computational domain.

Figure 5 shows the time evolution of the response for a case (C2) similar to case C1 (Fig. 4) except with $U = -9.5$ m s^{-1}. As can be seen from Fig. 5a, no positive total horizontal wind velocity exists in 10 h. That is, no reversed surface flow or stagnation point forms at the surface within 10 h. Therefore, no density current is able to form upstream. In this flow regime, the cold air outflow is overcome by the basic wind advection due to the wave reflection from the top boundary. Notice that a density current is able to form in a corresponding case with a sponge layer located at $z = 10$ to 15 km (Figs. 2b and 3d). The cold air produced by the evaporative cooling becomes almost stationary, as can be seen from Fig. 5c. However, the gravity waves are able to propagate both upstream and downstream (Figs. 5b and 5d). Obviously, this case belongs to the regime of critical to outflows and subcritical to gravity waves. In fact, this case corresponds to $(G, F) = (1.00, 1.14)$. The upstream-propagating gravity wave (wave I) is more evident in this case (Fig. 5b) than that in the last case (Fig. 4b).

The corresponding vertical structures of the disturbances at $t = 5$ h and $t = 10$ h are shown in Figs. 5e–f. At $t = 10$ h, the downstream outflow near the surface has already been advected out of the computational domain (Fig. 5e), while the cold region located near the cooling center is compensated by the adiabatic warming associated with stronger downward motion (Fig. 5f). The four-cell pattern of the vertical velocity shown in case C1 (Fig. 4f) becomes more widespread and is advected farther downstream in the present case (Fig. 5f). There exists no strong vertical motion in the vicinity of the cooling near the surface. This is because the flow is no longer subcritical to outflows. This is consistent with the finding of RR that strong updrafts only occur in the case of subcritical to outflows and supercritical to gravity waves. At $(x, z) = (82, 2 \text{ km})$, a region of upward motion can be found. This upward motion is associated with the propagating wave mode (wave I) as found in the previous case, except that it propagates upstream at a slower speed since the basic wind is stronger. In the vicinity of the cooling region, the stationary wave mode is dominated by downward motion. Therefore, this case may be classified to be *critical to outflows and subcritical to gravity waves.*

If we increase the basic wind velocity to -11 m s^{-1}, the response is quite dramatic. The result is shown in Fig. 6 (C3). The nondimensional flow parameters are $(G, F) = (1.15, 1.32)$. Since the wind speed is larger than the previous case, one would anticipate that a reversed flow and subsequently a density current would not be able to form, according to the theory of RR. Surprisingly, a reversed flow is able to form (Figs. 6a and 6b). A density current then forms at about the same time and propagates farther upstream as time

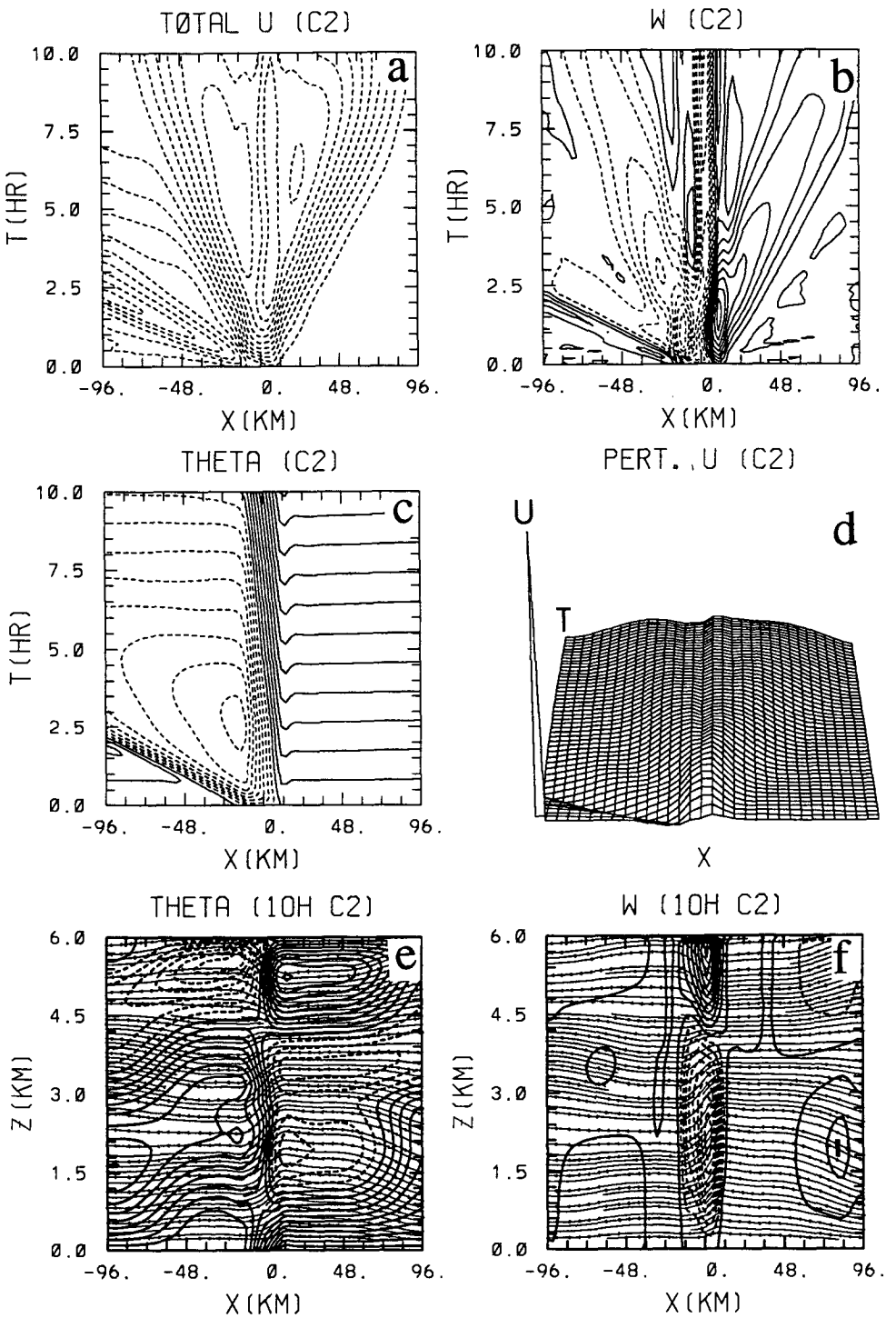

FIG. 5. (C2) Same as Fig. 4 except with $U = -9.5$ m s^{-1}. The θ and w fields are only depicted at 10 h [(e) and (f)]. The flow is critical to outflows but is subcritical to gravity waves. Notice that no density currents form in 10 h even though the basic wind is stronger than that in case C1. The contour intervals for (a), (b), (c), (e), and (f) are 0.4 m s^{-1}, 0.004 m s^{-1}, 0.1 K, 0.1 K, and 0.04 m s^{-1}, respectively.

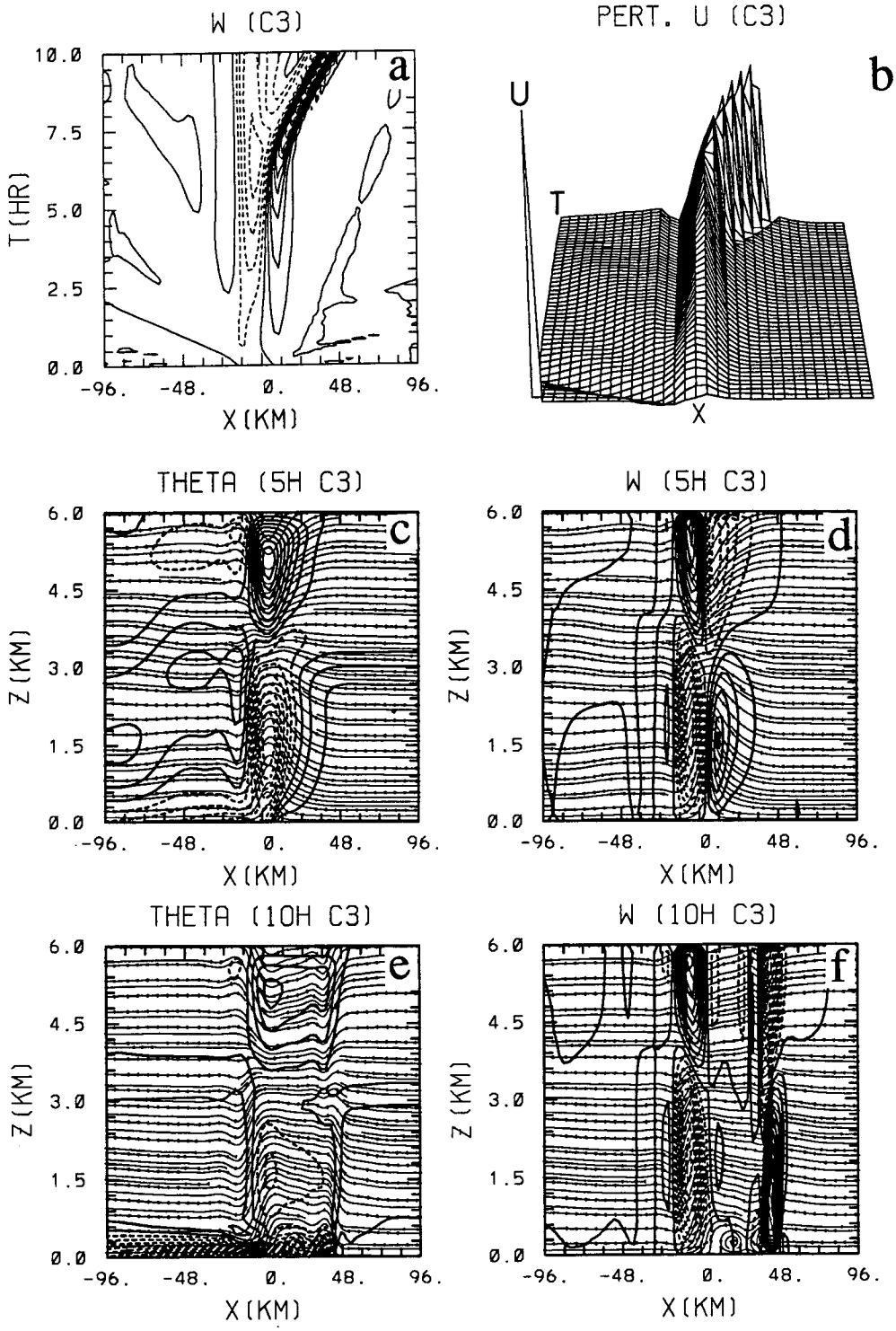

FIG. 6. (C3) Same as Fig. 4 except with $U = -11$ m s^{-1}. The time evolutions of w and 3D plot of u are shown in (a) and (b). The vertical structures with streamline fields are shown in (c) θ at 5 h, (d) w at 5 h, (e) θ at 10 h, (f) w at 10 h. The flow is critical to both outflows and gravity waves. The formation of the density current is due to the wave–outflow interaction. The contour intervals for (a), (c), (d), (e), and (f) are 0.03 m s^{-1}, 0.2 K, 0.1 m s^{-1}, 0.5 K, and 0.09 m s^{-1}, respectively.

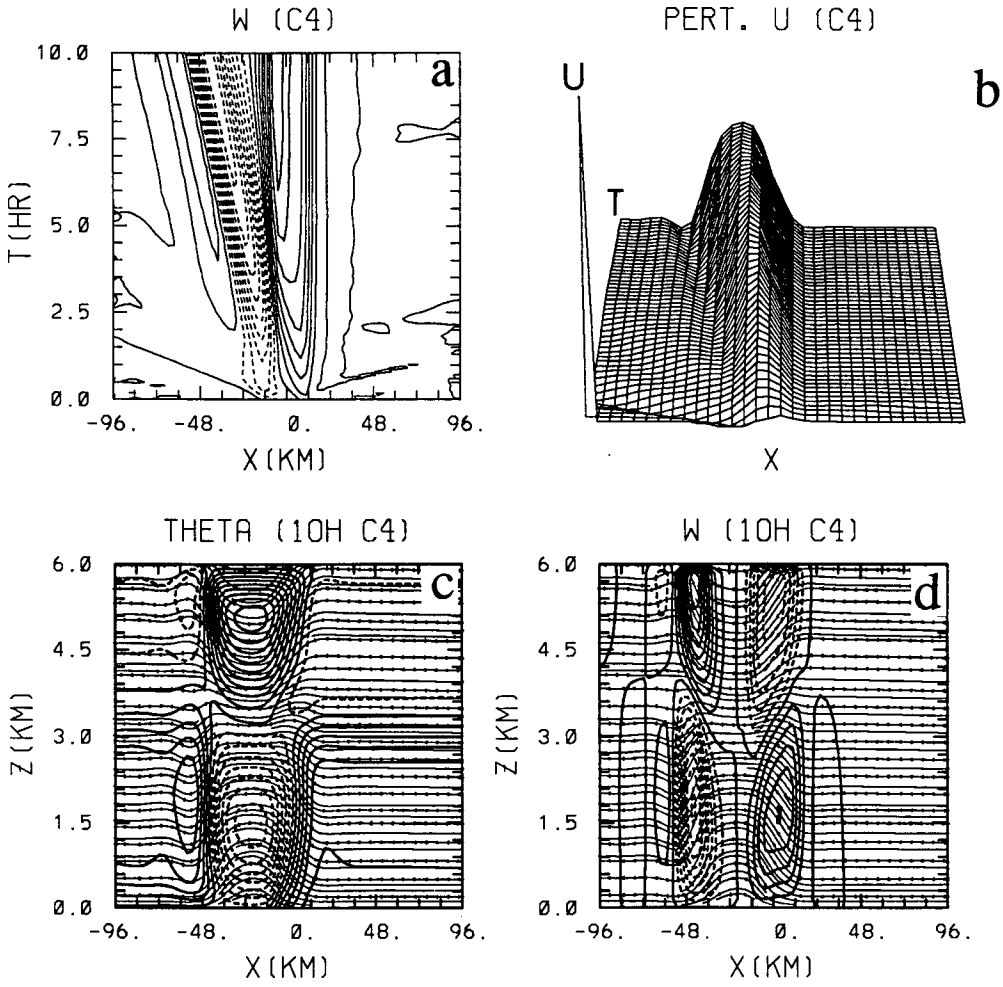

FIG. 7. (C4) Same as Fig. 4 except with $U = -13$ m s^{-1}. Four fields are shown: (a) time evolution of w at z = 150 m, (b) 3D plot of u at $z = 0$, (c) θ at 10 h, and (d) w at 10 h. The flow is supercritical to both outflow and gravity waves. The contour intervals for (a), (c), and (d) are 0.01 m s^{-1}, 0.2 K, and 0.08 m s^{-1}, respectively.

proceeds. The magnitude of this density current (Fig. 6b) is even larger than case C1 in which the basic flow was specified to be $U = -8$ m s^{-1} (Fig. 4d). It appears that the formation of this density current is due to the interaction between wave I and the cold air outflow. In the present case, wave I is advected to the area of the convergence zone produced by the prescribed cooling. In case C1 (Fig. 4), the upstream-propagating wave already propagates to a region near the right boundary. This indicates that the formation of the density current in case C1 is caused purely by the cold air outflow being able to push against the relatively weak basic wind. However, the density current in the present case forms as a result of the nonlinear interaction between two different sources of flow convergence near the surface. This interaction between the cold air outflow and the cooling-induced gravity wave is responsible for the existence of the anomaly in the critical curve (F_c) associated with the F–G parameter map (Figs. 2 and 3).

Figures 6c–f shows the vertical structure of the disturbances for case C3. As discussed above, the gravity wave is able to interact nonlinearly with the cold air outflow and generate a density current. This disturbance is categorized as a "gravity wave with stagnation" by Crook and Moncrieff (1988). The formation mechanism is quite different from that for case C1 (Fig. 4). This is clearly evident by comparing the vertical structures of Figs. 4 and 6. The cold region extends to a height of about 4 km in this case (Fig. 6c), instead of about 2 km in case C1 (Fig. 4e). This is an indication that the disturbance is strongly influenced by the propagating wave mode (wave I), which has a larger vertical wavelength, as also shown near $x = 72$ km in Fig. 4f. This gravity wave remains stationary and is located just upstream of the cooling region (Fig. 6d). The disturbance is dominated by upward motion upstream of the cooling center ($x > 0$ km), while the cold air region is dominated by

TABLE 2. Summary of numerical experiments with one heat source and/or one heat sink.

	Case		
	CH2/H2	CH3/H3	CH4/H4
	Figure		
	8	9	10
U (m s^{-1})	−9.5	−11	−13
cooling rate (J kg^{-1} s^{-1})	−0.3/0	−0.3/0	−0.3/0
cooling depth (km)	3	3	3
heating rate (J kg^{-1} s^{-1})	0.6	0.6	0.6
heating base (km)	2	2	2
heating top (km)	6	6	6
l (km)	18	18	18
N (s^{-1})	0.01	0.01	0.01
Fr	0.32	0.37	0.43
G	1.00	1.15	1.36
F	1.14	1.32	1.56

downward motion downstream. An alternative explanation of the formation of density current in the present case is as follows. A deeper region of cooling associated with the gravity wave is forced by the deeper updraft, which then couples with the cold outflow (unlike case C1) to form, in essence, a much deeper cold pool with an associated greater potential energy. The conversion of this greater potential energy to kinetic energy of the outflow would be accomplished as the cold air collapsed under the influence of gravity. However, this may imply that a density current should be able to form in case C2, which is not observed. Once the density current forms, it becomes very shallow, is confined to a depth of about 1 km, and propagates upstream at the same speed (Fig. 6e) as in case C1 (Fig. 4g). The gravity waves forced by the density current have a larger vertical wavelength (Fig. 6f) than that in case C1 (Fig. 4h) since the basic wind speed is stronger and the vertical wavelength of the gravity wave is inversely proportional to the Scorer parameter (N/U). The upward motion associated with this density current also extends to a higher level. The results indicate that this case may be classified to be subcritical to outflows and critical to gravity waves, although it should be regarded as *critical to both outflows and gravity waves* since both the cold air outflow and wave I are stationary in the vicinity of the cooling region before the outflow–wave interaction.

Figure 7 shows the time evolution of the flow response for a case (C4) similar to case C3 (Fig. 6) except with $U = -13$ m s^{-1}. The nondimensional flow parameters are (G, F) = (1.36, 1.56). In this case, no reversed flow or stagnation point forms within 10 h. Since the basic wind speed is stronger, the cold air outflow does not have enough momentum to push against the basic flow. The flow response obviously falls into the category of supercritical to outflows. In addition, it is important to notice that wave I (wave upstream propagating in a weaker environmental flow) is now being advected to the downstream side of the cooling region by the basic flow (Fig. 7a). This makes it impossible for the interaction between the cooling-induced gravity waves and the outflow to occur, such as that occurs in case C3 (Fig. 6). Even though upward motion still exists in the vicinity of the cooling region, the convergence is not strong enough to produce a reversed flow against the basic current. This is evident from Fig. 7b. The perturbation potential temperature field is similar to case C2 (Fig. 5c) except that a stronger temperature gradient now exists on the downstream side of the cooling region. Even though there exists no stagnation point or reversed flow in this case, the perturbation horizontal velocity (Fig. 7b) is much stronger than that in case C2 (Fig. 5d).

The vertical structure of the disturbances at $t = 10$ h is shown in Figs. 7c–d. At $t = 5$ h, the flow response as evidenced in the potential temperature field and the vertical velocity field (not shown) is similar to the previous case (Figs. 6c and 6d). However, these patterns are shifted farther downstream to a distance of $x = -15$ km in the present case, instead of being located at the cooling center ($x = 0$ km) as in the previous case. At $t = 10$ h, wave I is being advected farther downstream (Figs. 7c and 7d). This provides evidence, along with the time evolution fields (Figs. 7a and 7b), that both the cold air outflow and wave I are advected downstream by the stronger basic wind. Therefore, this case falls into the category of *supercritical to both outflows and gravity waves* according to the classification proposed by RR. Notice that the air ascends over the cooling region, as found by Smith and Lin (1982) and explained in Lin and Smith (1986). It is also discussed in Thorpe et al. (1980) and may be classified as the "jump" type of flow associated with thunderstorm downdrafts. This type of disturbance, categorized as a solitary gravity wave by Dudhia et al. (1987), has no stagnation point.

5. Interactions between gravity waves and cold air outflows

In the last section, we have found that the upstream-propagating gravity waves (wave I) produced by the prescribed cooling can be advected by the basic wind and interact nonlinearly with the cold air outflow when wave reflections from upper levels exist. This wave–outflow interaction, in turn, is able to generate a reversed surface flow or stagnation point that makes it possible for a density current to develop. The density current then propagates against the basic flow. Based on this interesting finding, we hypothesize that *the wave–outflow interaction will take place between a traveling gravity wave and a cold air outflow when wave reflections exist from above.*

a. Flow over a heat sink and a heat source

To test this hypothesis, we have performed several numerical experiments with prescribed heating, in addition to the cooling. The numerical simulations with heating and/or cooling performed in this section are summarized in Table 2. The heating is used only to provide a mechanism for generating gravity waves in the vicinity of the cooling region. This provides a simple way to examine if any interactions exist between the traveling gravity wave and the cold air outflow. Figures 8a and 8b show the time evolutions of the vertical velocity at $z = 150$ m and the perturbation horizontal velocity at the surface for a stably stratified, uniform flow passing through a prescribed heating region (H2). The basic wind velocity is -9.5 m s^{-1}. The heating is turned on at $t = 0$ s and forces the basic state flow at a constant rate of 0.6 J kg^{-1} s^{-1} for only 2 h. The heating region is located between 69 km $< x <$ 87 km and 2 km $< z <$ 6 km. In the first 2 h, the response of the flow to heating is dominated by the forced gravity wave, which is composed of a stationary mode and a propagating mode. Even though only the mode propagating downstream is shown, a mode propagating upstream should also exist. The heating generates upward motion just downstream of the heating center ($x = 78$ km). This response is similar to the results of Lin and Smith (1986). The downstream-propagating mode has a relatively smaller amplitude compared to the stationary mode. The disturbance behaves differently after 2 h since the heating is turned off suddenly at $t = 2$ h. The primary gravity wave is propagating slowly to the downstream side of the heating region. Figures 8c and 8d show the same fields except for the case of combined cooling and heating (CH2). Surprisingly, with both a low-level cooling and an elevated heating added to the system, a density current is able to form at about $t = 5$ h. Notice that no density current can form in the corresponding cooling case (C2, Fig. 5). The time evolution of the vertical velocity at $z = 150$ m behaves very differently from the corresponding cooling case. The convergence zone associated with the heating-induced gravity wave is able to add to and interact nonlinearly with the convergence zone associated with the cold air outflow produced by the prescribed cooling. This nonlinear interaction appears to be responsible for producing the strong upward motion and reversed flow. Once the density current forms, the flow becomes strongly nonlinear and tends to feed back to the basic state. The wave structure downstream of the prescribed cooling region is totally different from the corresponding cooling case (C2). Instead, the vertical velocity field looks more like the cooling case with $U = -8$ m s^{-1} (C1, Fig. 4).

Figures 8e–h depicts the vertical structure of the perturbation potential temperature field at the surface and the vertical velocity at $z = 150$ m for case CH2 at $t = 5$ h and $t = 10$ h. Both the potential temperature and vertical velocity fields are significantly different from the corresponding cooling case (case C2, Fig. 5). At $t = 5$ h, the temperature gradient upstream of the cooling center near the surface is much stronger than that in C2 since a warm region associated with the traveling wave generated by the heating exists. This is also evident from the cold air located at $x = 48$ km. Above the cooling region, the flow is dominated by warm air. A region of very warm air is located at $x = -50$ km near the upper boundary, which is due to wave reflection. A region of upward motion forms upstream of the cooling center at $t = 5$ h and another region forms at $(x, z) = (-18, 3.5$ km) (Fig. 8f). The vertical structure of the vertical velocity is similar to the cooling case with $U = -8$ m s^{-1} (C1, Fig. 4f).

In cases H3 and CH3, the basic wind velocity is -11 m s^{-1}. The time evolution of the vertical velocity at $z = 150$ m and the perturbation horizontal velocity at the surface for a stably stratified, uniform flow passing over a prescribed heating region (H3) are very similar to the previous case (Figs. 8a and 8b) except that stronger downstream advection exists due to the stronger basic wind. Figures 9a and 9b show the same fields except for a combined cooling and heating (CH3). The cooling is stationary, while the heating lasts for just 2 h as in case H2. These fields should be compared with case C3 (Figs. 6a and 6b). Notice that the disturbance near the cooling center is suppressed almost completely by the downstream-traveling gravity wave. Unlike the previous case, the stationary gravity wave mode forced by cooling interacts with the primary wave produced by heating in a negative sense. It appears that the divergence zone associated with the heating-induced gravity wave tends to reduce the convergence zone located just upstream of the cooling center. Notice that the convergence zone in case C3 is associated with both the upstream-propagating gravity wave (wave I) and the cold air outflow in the cooling case (case C3). This process, in turn, weakens the upward motion in the present case. By comparing Figs. 6a and 9a, the interaction of gravity waves and outflows is wholly nonlinear, and not a simple linear superposition of both disturbances.

Figures 9c–d depict the vertical structure of the disturbances for case CH3 at $t = 10$ h. The cold area is widened and extends farther upstream of the cooling center compared with the corresponding cooling case (C3, Figs. 6c–f). The widening of this cold area is due to the adiabatic cooling associated with the upward motion. Therefore, the temperature gradient and convergence near the cooling center are weakened. The whole structure looks more like the cooling case with $U = -9.5$ m s^{-1}. In the present case, wave I is able to propagate upstream (Figs. 9c and 9d). Thus, the disturbance falls into the regime of *critical to outflows and subcritical to gravity waves.* In other words, the flow response tends to shift to another regime by the inter-

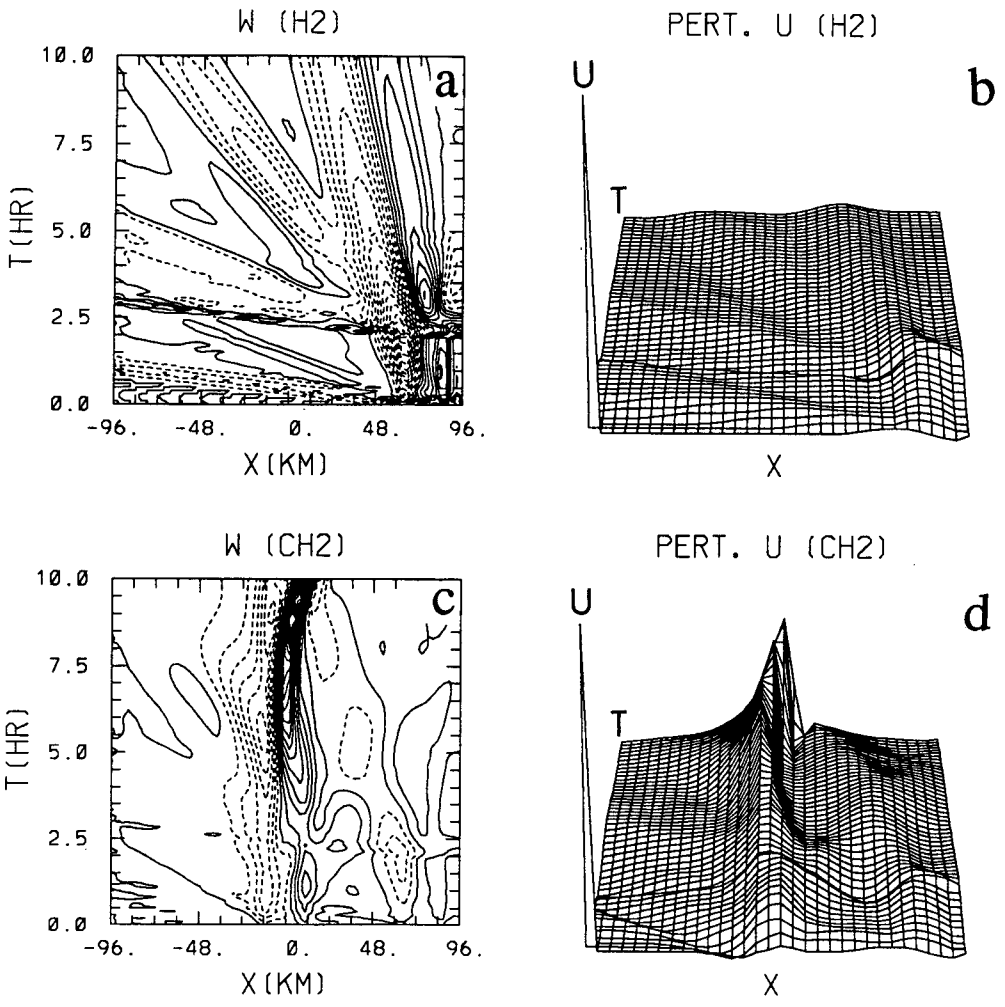

FIG. 8. Time evolution of the response for a stably stratified uniform flow passing over a heat source (H2) and a heat sink and a heat source (CH2). The basic wind velocity is -9.5 m s^{-1}. The cooling and heating rates are -0.3 J kg^{-1} s^{-1} and 0.6 J kg^{-1} s^{-1}, respectively. The cooling extends from the surface to 3 km, and the heating base and top are 2 and 6 km, respectively. The width of both the cooling and heating is 18 km. The cooling is stationary, while the heating lasts only for 2 h. Other flow parameters are the same as in the corresponding cooling case (C2). Four fields of time evolution are shown: (a) w at z = 150 m (H2), (b) 3D plot of u at

action between the gravity waves and the cold air outflow.

In cases H4 and CH4, the basic wind velocity is -13 m s^{-1}. The time evolution of the vertical velocity at z = 150 m and the perturbation horizontal velocity at the surface is similar to case H2 (Figs. 8a and 8b). However, the primary gravity wave produced by the heating propagates downstream at a faster speed since the basic wind is stronger. The flow response due to combined cooling and heating is shown in Figs. 10a and 10b (CH4). Surprisingly, with both cooling and heating added to the system, a density current is able to form at about t = 5 h. Notice that no density current can form in the corresponding cooling case (C4, Fig. 7). The time evolution of the vertical velocity at z = 150 m behaves very differently from the corresponding cooling case. The convergence zone associated with the heating-induced gravity wave is able to interact nonlinearly with the convergence zone associated with the cold air outflow produced by the prescribed cooling. This nonlinear interaction appears to be responsible for producing the strong upward motion and then the reversed flow. Once the density current forms, the flow becomes strongly nonlinear and tends to modify the basic state. The wave structure downstream of the prescribed cooling region is totally different from the corresponding cooling case (C4). Instead, the vertical velocity field looks more like the cooling case with $U = -11$ m s^{-1} (C3, Fig. 6).

The major difference between the potential temperature field from the corresponding cooling case

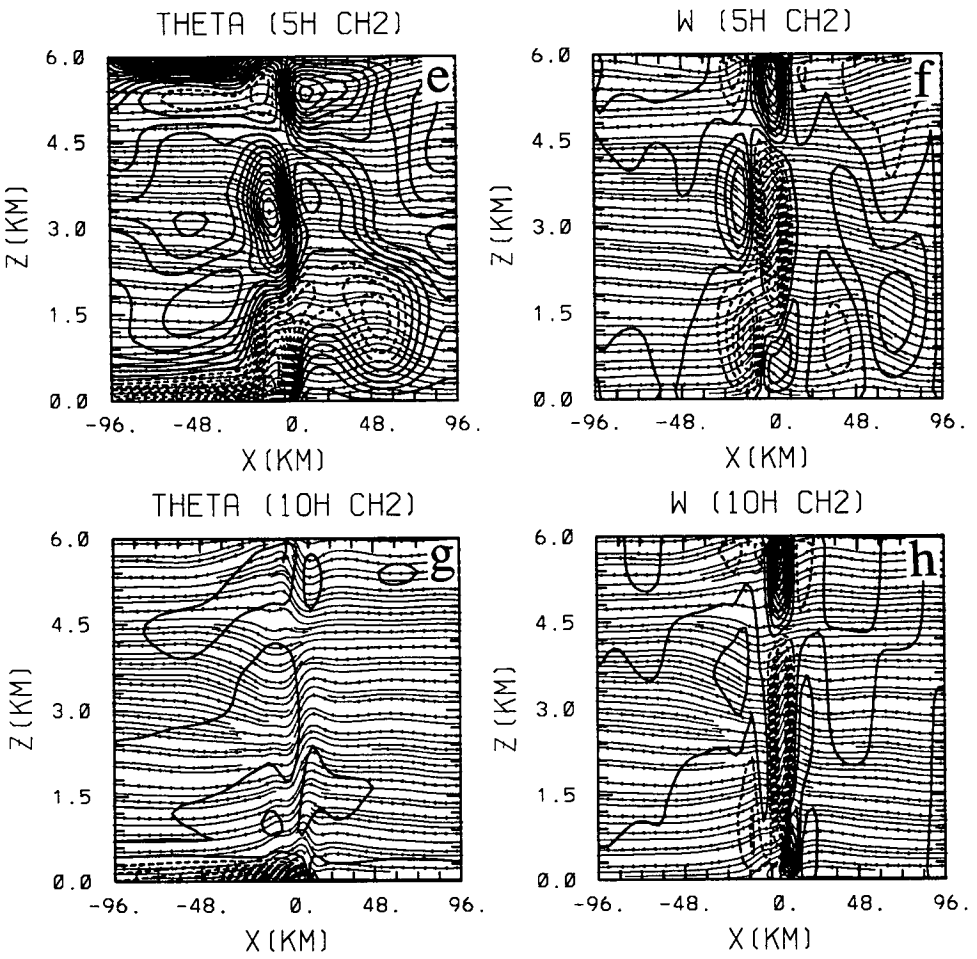

FIG. 8. (*Continued*) $z = 0$ (H2), (c) w at $z = 150$ m (CH2), (d) 3D plot of u at $z = 0$ (CH2). The vertical structures with streamlines imposed for case CH3 are shown in (e) θ at 5 h, (f) w at 5 h, (g) θ at 10 h, (h) w at 10 h. Notice that a density current is able to form by the wave–outflow interaction, which is not able to form in the corresponding case (C2). The contour intervals for (a), (c), (e), (f), (g), and (h) are 0.002 m s^{-1}, 0.01 m s^{-1}, 0.1 K, 0.04 m s^{-1}, 0.6 K, and 0.06 m s^{-1}, respectively.

(C4, Fig. 7) at an earlier time, for example, 5 h, is that the cold region is located near the cooling center, instead of being advected downstream. This cold region is anchored to the cooling region since it is prevented from being advected downstream by the interaction between the convergence zone produced by the heating and that produced by the cooling. The vertical structure of the disturbance is similar to the cooling case with $U = -11$ m s^{-1} (C3, Fig. 6).

The interaction between the gravity wave and cold air outflow is highly dependent on the relative location and strength of the prescribed heat source and sink or the phase relationship between them. In other words, the interaction may be destructive or constructive, such as demonstrated in the above two examples. In addition, a stronger cooling or heating tends to introduce stronger interactions.

b. Flow over two heat sinks

It is crucial to examine the above mechanism of interactions between gravity waves and outflows when two nearby heat sinks exist. Figure 11 shows the response of a stably stratified quiescent fluid to two heat sinks (CC0) when wave reflections exist from above. As in previous cases, a rigid lid is placed at 6 km. The heat sinks are located at $x = -24$ and $x = +24$ km and have a cooling rate of -0.3 J kg^{-1} s^{-1}. Other flow parameters are the same as those in case C1 except with $U = 0$ m s^{-1} and are summarized in Table 3. In the beginning, each heat sink produces its own cold air outflow that propagates outward from the cooling center. At the center of the domain ($x = 0$ km), the two outflows collide with each other. After the collision, the two outflows weaken and form a single region of cold air and upward motion, which is then stationary

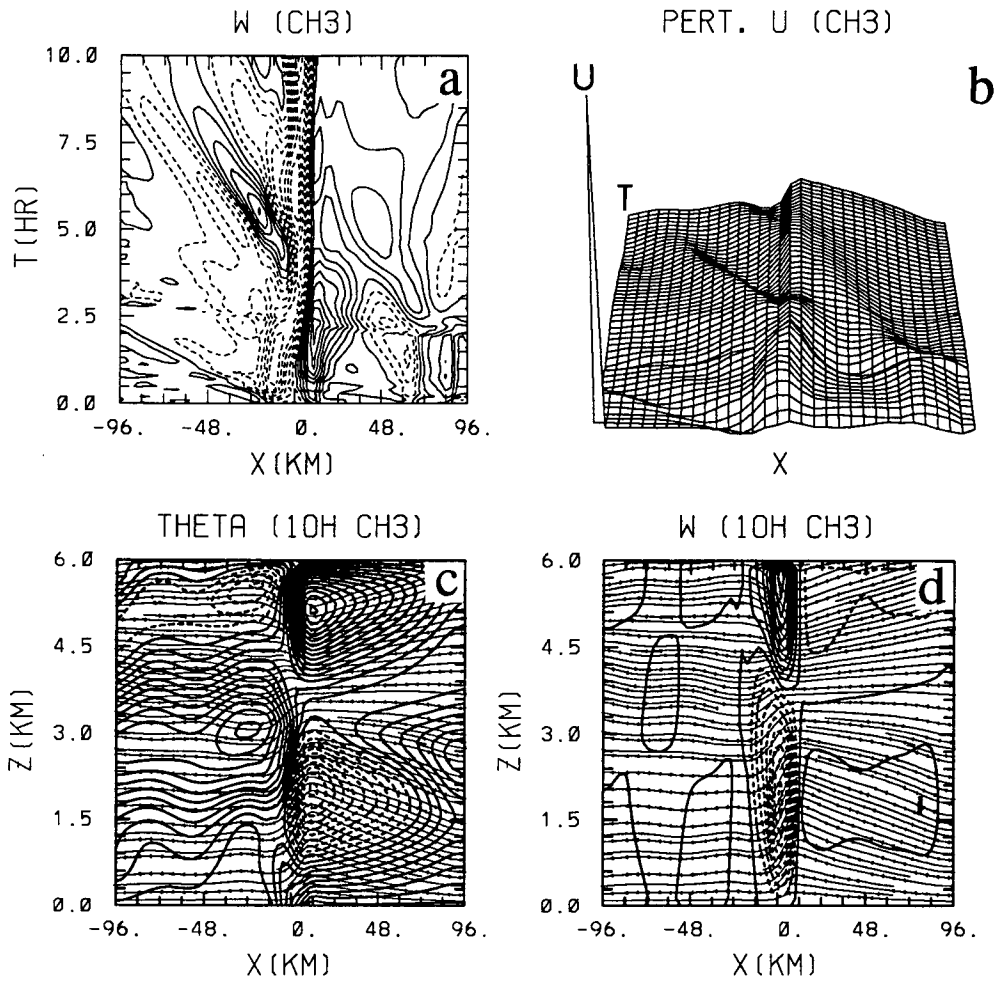

FIG. 9. (H3 and CH3) Same as Fig. 8 except with $U = -11$ m s^{-1}. Four fields are shown: (a) time evolution of w at $z = 150$ m, (b) 3D plot of u at $z = 0$, (c) θ at 10 h, and (d) w at 10 h. The density current in the corresponding case (C3) is wholly suppressed by the wave–outflow interaction. The contour intervals for (a), (c), and (d) are 0.005 m s^{-1}, 0.1 K, and 0.06 m s^{-1}, respectively.

at this location within the computational domain at later times. This behavior is indicative of material flows, and is quite different from that of gravity waves, which tend to pass through each other. A narrow region of convergence and upward motion is associated with the merger of outflow boundaries (Fig. 11a). The upward motion is supported by the convergence generated by the continuous cooling. At a fixed point located outside the heat sinks near the surface, the potential temperature decreases gradually when the cold air outflow passes over it. This behavior is different from that of the passage of a density current, which has a narrow region of sharp temperature gradient (e.g., see Fig. 4c). With a nonhydrostatic model, this temperature gradient should be stronger. This phenomenon is similar to that found in the quiescent fluid case of Droegemeier and Wilhelmson (1985a,b). However, it is noteworthy to point out that the magnitude of the vertical velocity associated with this new cold air region reaches its maximum at about 2.5 h and then decreases gradually with time, even though the magnitude of the prescribed coolings is kept constant throughout the simulation. This decay is caused by the combination of downward motions associated with the gravity waves forced by the prescribed coolings. Notice that these two gravity waves are reflected back from the top boundary. In other words, an interaction exists between the thermally forced gravity waves and cold air outflows.

The vertical structures of the potential temperature field at the surface and vertical velocity at $z = 150$ m at $t = 1$ h and $t = 2$ h are shown in Figs. 11c–f. At $t = 1$ h, the lower layer is occupied by a pool of cold air with maxima located at the cooling centers. A compensated warm region forms in the upper layer as required by mass continuity. At this time, upward-propagating gravity waves exist in the upper layer, although

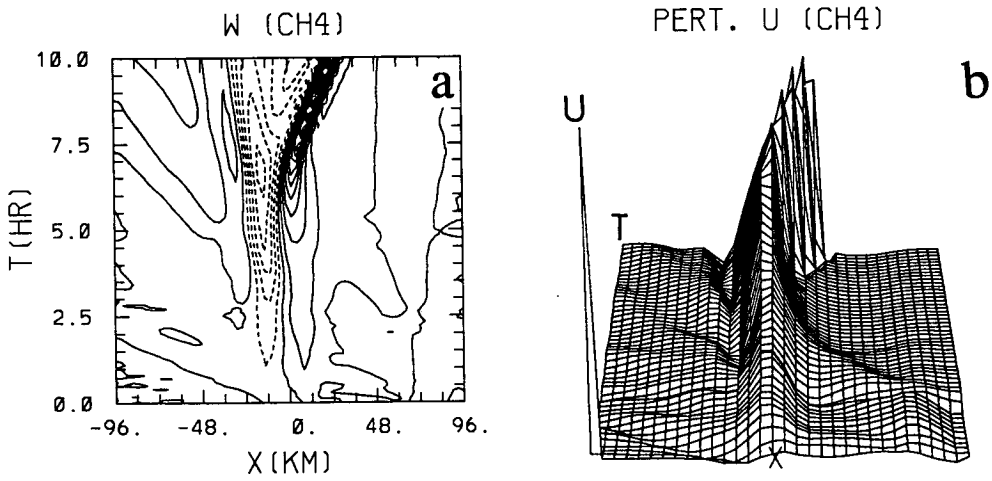

FIG. 10. (H4 and CH4) Same as Fig. 8 except with $U = -13$ m s^{-1}. Only two fields of time evolution are shown: (a) w at $z = 150$ m, and (b) 3D plot of u at $z = 0$. A density current is able to form by the wave–outflow interaction, which is not able to form in the corresponding case (C4). The contour interval for (a) is 0.02 m s^{-1}.

some of them have already been reflected back from the rigid lid (Figs. 11c and 11d). Near the cooling regions, the flow response is dominated by downward motion (Fig. 11d), as expected. Compensative upward motions are produced by the cooling, which propagate outward from each cooling center. At the center of the coupled heat sinks, these two regions of upward motion interact with each other and generate a single region of stronger upward motion. This is associated with the collision process. At $t = 2$ h, the cold air near the cooling centers descends farther to the surface (Fig. 11e). The two regions of upward motion continue propagating outward. The upward motion near $x = 0$ km strengthens but is confined in a very shallow layer below 1 km (Fig. 11f). A comparison of Figs. 11d and 11f shows that the upper portion of the upward motion region at 1 h is suppressed by the downward motions, which are associated with outward-propagating gravity waves generated by the continuous coolings. It appears that it is unlikely that new convection can be triggered by such a shallow layer of upward motion.

In order to investigate the impact of this wave–outflow interaction on a stably stratified uniform flow passing over two heat sinks, we have performed two additional experiments. The flow parameters of these experiments are summarized in Table 3. Figure 12 shows the time evolution of the vertical velocity at $z = 150$ km and the perturbation horizontal velocity for a case (CC1) similar to the previous case except with $U = -8$ m s^{-1}. This figure may be compared with Fig. 4 (C1). With only one heat sink, a density current forms at about $t = 5$ h and propagates against the basic flow (Fig. 4). It can be seen from the figure that two density currents (density currents L and R) are formed individually by these two heat sinks at about the same time. However, a new density current, denoted by N in the figure, develops on the upstream (right) side of the right heat sink. Density current N originates from the right heat sink but then splits from density current R at later times. Density current R forms earlier and is weaker than the corresponding case with one heat sink (C1, Fig. 4d), while density current L forms later and is much weaker. In fact, density current L is suppressed significantly by the downward motion and divergence zone associated with the gravity wave forced by the upstream prescribed heat sink. Density current N is formed by the interaction between the upstream-propagating waves forced by the left heat sink and the cold air outflow associated with the right heat sink. This process is clearly depicted in the vertical structure of the disturbances at $t = 5$ h as shown in Figs. 12c and 12d. It is interesting to note that the general patterns of the potential temperature perturbation and upward motion near the left heat sink ($x = -24$ km) in the present case (Figs. 12e and 12f) are similar to the corresponding case (C1, Figs. 4e and 4f). However, the region of upward motion centered at $(x, z) = (50, 1$ km) is nonlinearly enhanced by the upward motion associated with the right heat sink and the upstream-propagating wave mode (wave I) produced by the left heat sink. This is evidenced by inspecting Fig. 4f, which shows that wave I produced by the left heat sink has already traveled to a distance of 72 km from the heat sink (Fig. 4f). This upstream-propagating wave produced by the left heat sink is able to propagate through the cold air outflow or density current produced by the right heat sink since it has a higher phase speed. The associated upward motion tends to help develop density

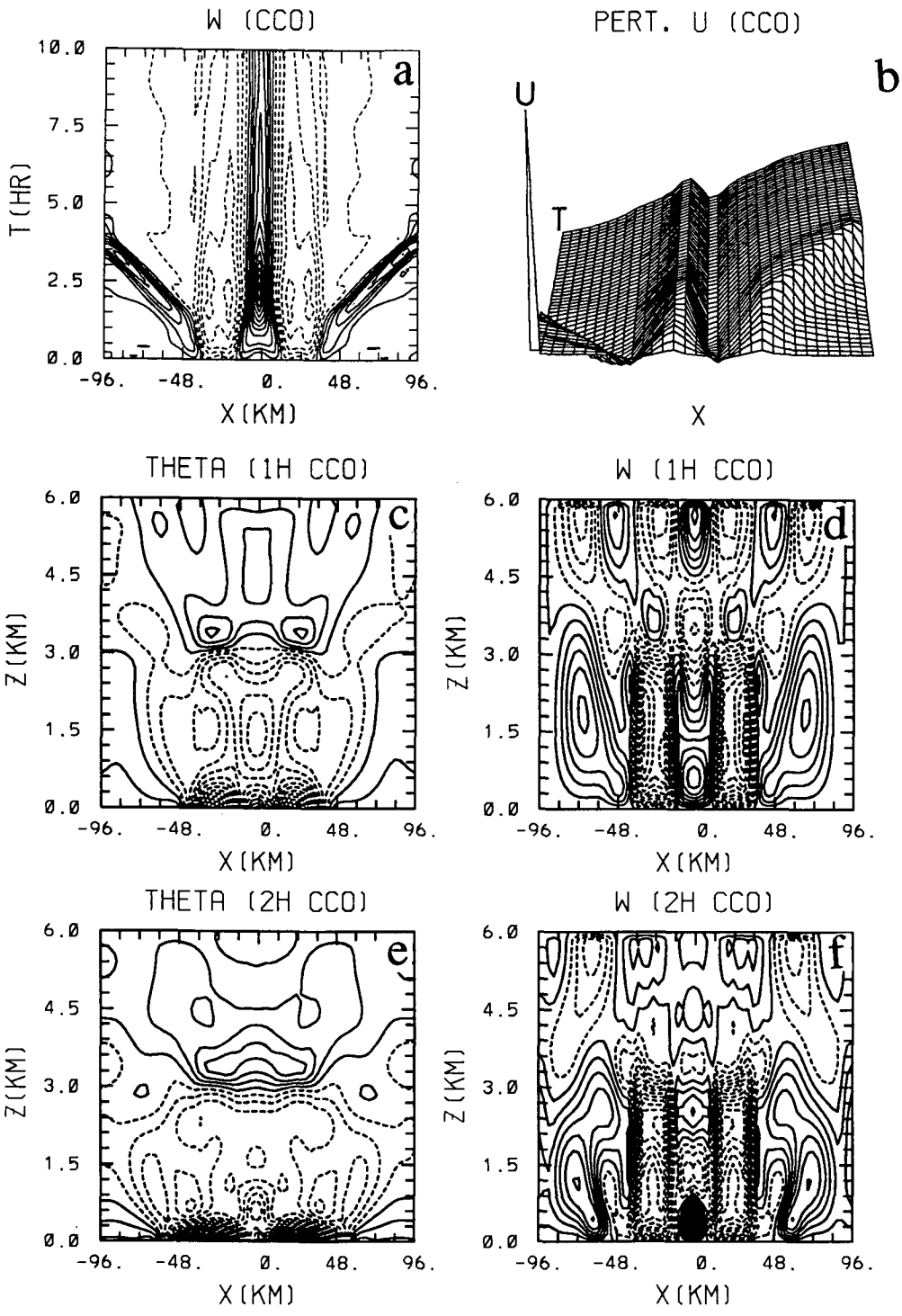

FIG. 11. (CC0) Time evolutions of the response for a stably stratified fluid to two stationary coolings (l = 18 km, d = 3 km). The cooling rate is -0.3 J kg^{-1} s^{-1} for both heat sinks, which are 48 km apart. Other flow parameters are listed in Table 3. The time evolutions of w at z = 150 m and 3D plot of u at z = 0 m are shown in (a) and (b), respectively. The vertical structures are shown in (c) θ at 1 h, (d) w at 1 h, (e) θ at 2 h, and (f) w at 2 h. At x = 0, the cold air outflows collide and merge into a stationary one that gradually weakens from the influence of gravity waves. The contour intervals for (a), (c), (d), (e), and (f) are 0.008 m s^{-1}, 0.08 K, 0.01 m s^{-1}, 0.1 K, and 0.01 m s^{-1}, respectively.

TABLE 3. Summary of numerical experiments with two heat sinks.

	Case		
	CC0	CC1	CC2
	Figure		
	11	12	13
U (m s^{-1})	0	−8	−9.5
Q_0 (J kg^{-1} s^{-1})	−0.3	−0.3	−0.3
l (km)	18	18	18
d (km)	3	3	3
N (s^{-1})	0.01	0.01	0.01
Fr	0	0.27	0.32
G	0	0.84	1.00
F	0	0.96	1.14

current N. This new density current keeps developing and splits away from density current R, while density currents L and R develop gradually after t = 5 h (Figs. 12e and 12f). The downstream cold air region then joins the cold air associated with the upstream density currents. This indicates that the density current produced by a heat sink can be suppressed or enhanced by the gravity wave produced by a nearby heat sink. Again, this interaction is highly dependent on the relative location and strength of the prescribed heat sinks or the evaporative cooling associated with two nearby thunderstorm downdrafts. This process may have an important impact on cloud interactions since they are related to the interaction of two nearby thunderstorm downdrafts (Simpson 1980; Tao and Simpson 1984). We have performed a case with two heat sinks separated by 60 km (not shown). Results show that interactions do not occur strongly and that these density currents are able to preserve their own identities.

Figure 13 shows the response of a case (CC2) similar to the previous case except with $U = -9.5$ m s^{-1}. As discussed earlier in the last section (case C2), the flow falls into a regime critical to outflows and subcritical to gravity waves. Thus, wave I is able to propagate upstream, while the outflow is stationary with respect to the prescribed cooling. No density current is able to form in such a flow over only one heat sink in 10 h. However, a density current is able to form at about t = 5 h for such a flow over two nearby heat sinks (Figs. 13a and 13b). The heat sinks are separated by a distance of 48 km. The mechanism responsible for the formation of this density current appears to be a constructive wave–outflow interaction. This interaction is well depicted by the vertical structure of the disturbances at t = 5 h (Figs. 13c and 13d). The cold air regions produced by these two prescribed heat sinks join each other to form a rather broad region of cold air enclosed by these two heat sinks (Fig. 13c). The vertical velocity field shows that the upstream-propagating gravity wave (wave I) produced by the left heat sink is able to propagate through the cold air produced by the right heat sink. Although most of the upward motion of this gravity wave is compensated by the stronger downward motion associated with the stationary cold air outflow of the right heat sink, a region of upward motion can still be detected near (x, z) = (44 km, 2 km) (Fig. 13d). This region of upward motion then interacts nonlinearly with the cold air outflow associated with the right heat sink and generates the density current that forms at a later time and propagates upstream (Figs. 13e and 13f). Therefore, the wave–outflow interaction can be constructive, such as the present case, or destructive, such as the previous case.

6. Concluding remarks

The interactions between gravity waves and cold air outflows generated in a stably stratified uniform flow over various configurations and combinations of diabatic heat sinks and sources were studied using a simple two-dimensional nonlinear numerical model. With a large number of nonlinear numerical experiments, we have found that the critical curve F_c (RR) for the formation of a stagnation point or reversed surface flow in a stably stratified uniform flow over a prescribed cooling is not necessarily a simple smooth monotonic curve when wave reflection from the upper levels exists. That is, the formation time does not always increase as the Froude number or basic wind speed increases for a fixed cooling rate. In addition, the critical curve on the F–G map is also a function of the integration time. This anomaly is not evident for rather short numerical integration times ($t \leq 2.8$ h). For cooling rates of $Q_0 = -0.7$ to -4.0, some critical Fr exists below which little effect on the time of flow reversal is seen for increasing Fr but above which further increases of Fr quickly prevent flow reversal.

In the case with $U = -8$ m s^{-1} and $Q_0 = -0.3$ J kg^{-1} s^{-1} (C1), which is subcritical to both outflows and gravity waves, both the cold air outflow and gravity wave are able to propagate upstream, as found in RR. The cold air outflow then develops into a density current at later times. The stationary wave mode associated with the prescribed heat sink has a vertical wavelength of twice the cooling depth, while the upstream-propagating gravity wave mode has a larger vertical wavelength. Once the density current forms, a gravity wave is generated and travels with it. When the basic wind velocity increases to -9.5 m s^{-1} (C2), no stagnation point or reversed surface flow is able to form within 10 h. The propagating gravity wave mode (wave I) is able to propagate upstream from the cooling region. The cold air outflow becomes stationary and the cooling effect is compensated by the basic wind advection due to the wave reflection from upper levels. In the

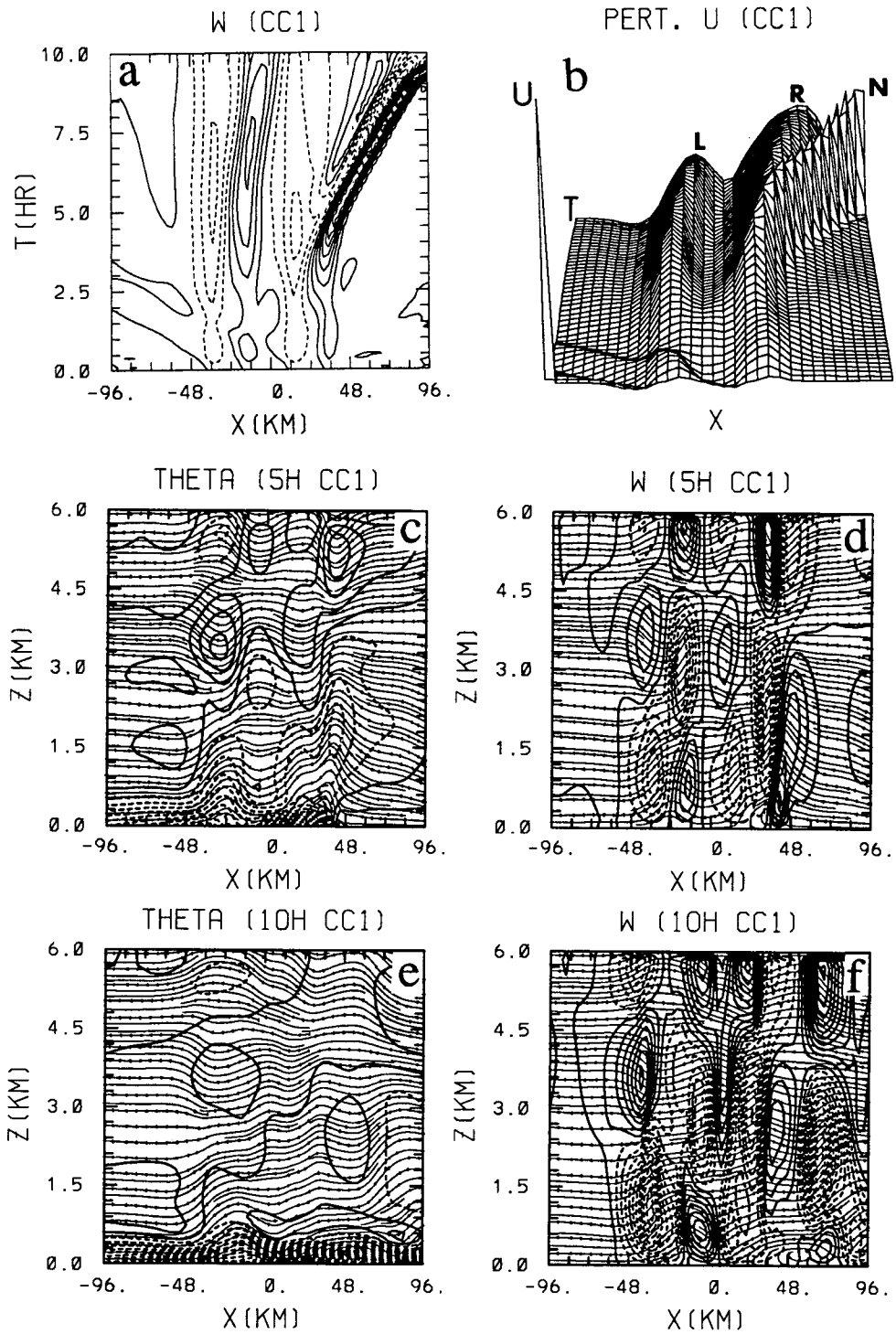

FIG. 12. (CC1) Same as Fig. 11 (case CC0) except with a uniform basic wind of -8 m s^{-1}. The left, right, and new density currents are denoted by L, R, and N, respectively. Notice that a new density current (N) is formed, while density current L is strongly suppressed and R is suppressed slightly. The contour intervals for (a), (c), (d), (e), and (f) are 0.02 m s^{-1}, 0.3 K, 0.05 m s^{-1}, 0.6 K, and 0.02 m s^{-1}, respectively.

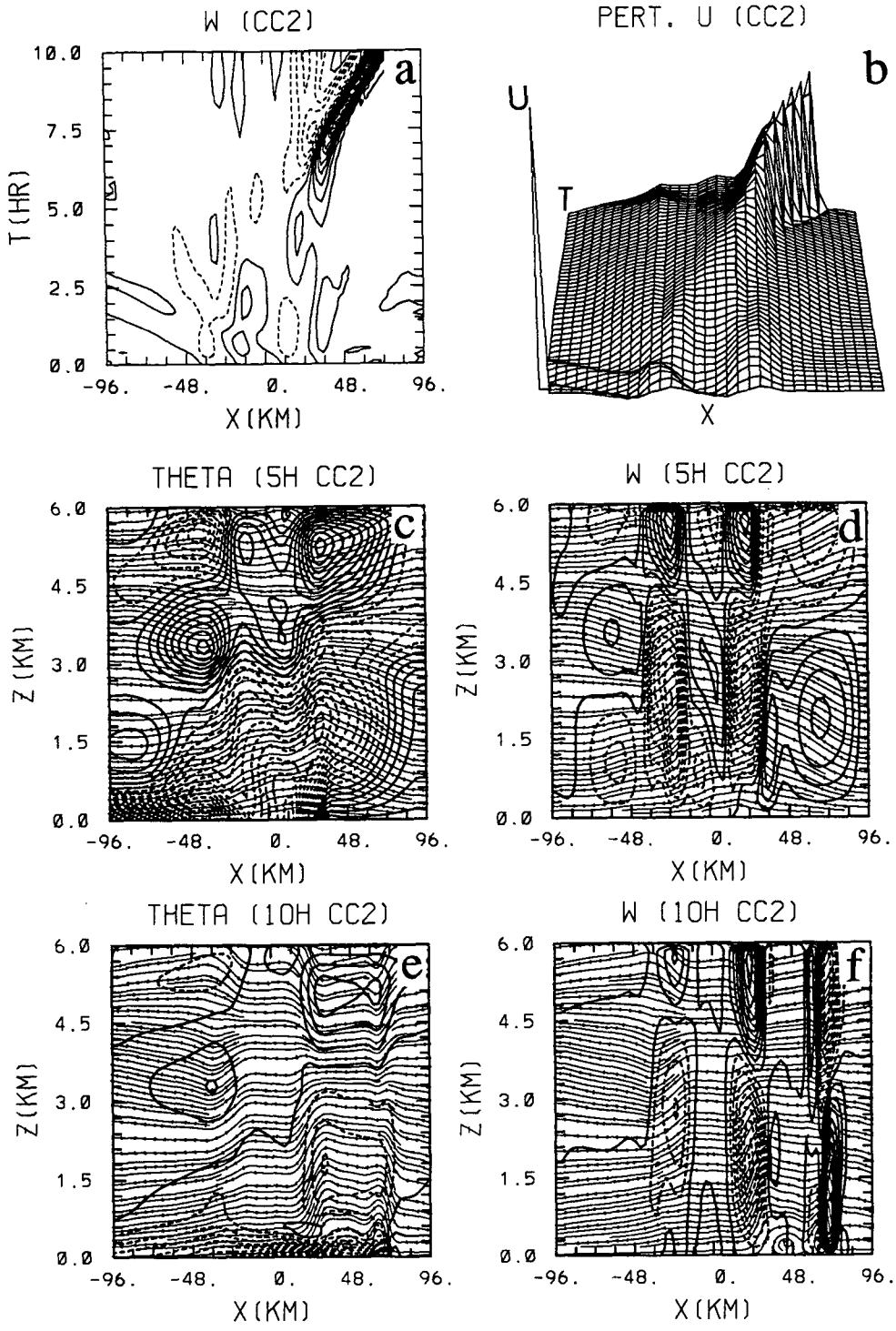

FIG. 13. (CC2) Same as Fig. 11 except with $U = -9.5$ m s^{-1}. A density current is able to form, which does not form in a flow over only one heat sink (C2). The contour intervals for (a), (c), (d), (e), and (f) are 0.02 m s^{-1}, 0.1 K, 0.03 m s^{-1}, 0.5 K, and 0.07 m s^{-1}, respectively.

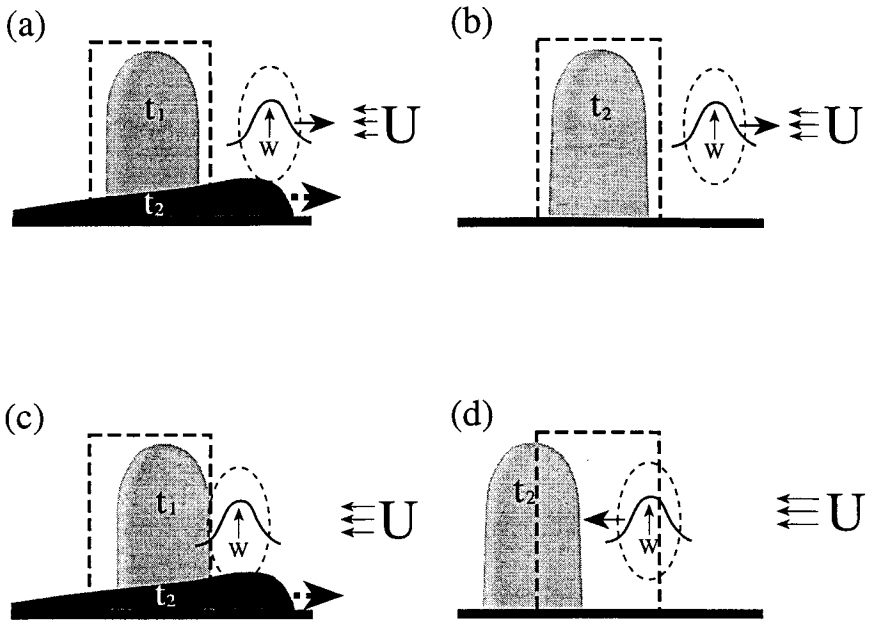

FIG. 14. A schematic diagram of flow responses and the interaction between gravity waves and cold air outflows in a two-dimensional stratified fluid flow passing a heat sink with the presence of wave reflection from the top boundary. (a) Subcritical to both outflows and gravity waves: both gravity waves and density currents are able to form and propagate upstream. The cold air has enough momentum to push against the basic flow. (b) Critical to outflows and subcritical to gravity waves: a gravity wave is able to form and propagate upstream, but no density current is able to form. (c) Critical to both outflows and gravity waves: a stationary gravity wave is able to form just upstream of the cooling region. A density current is able to form by the interaction between the cold air outflow and the gravity wave. (d) Supercritical to both outflows and gravity waves: the gravity wave propagates downstream. No density current is able to form. The region enclosed by bold dashed lines denotes the cooling region, while the region enclosed by elliptic dashed lines denotes the region of gravity wave disturbance. The cold pool is lightly shaded, while the density current is heavily shaded. The symbols t_1 and t_2 indicate an early stage and a later stage in the development, respectively.

vicinity of the cooling region, the quasi-steady-state flow is dominated by downward motion.

The downstream advection of the upstream-propagating gravity wave mode (wave I) has a strong impact on the flow response when the basic wind velocity increases to -11 m s^{-1} (C3). A density current is able to form in this case since wave I is located just upstream of the cold air outflow region. This nonlinear wave–outflow interaction provides a mechanism for enhancing the convergence and upward motion, which helps to form a reversed flow. This reversed flow then develops into a density current. The anomaly in the critical curve (F_c) on the F–G parameter map is due to this wave–outflow interaction. We classify this case as critical to both outflows and gravity waves since both are stationary with respect to the cooling at early times. If the basic wind velocity is increased to -13 m s^{-1} (C4), wave I is advected downstream of the cooling region. Therefore, the wave–outflow interaction does not occur and no density current is able to form. The flow responses and interaction between the gravity waves and cold air outflows are sketched in Fig. 14.

Based on the above findings, it was hypothesized that a density current may be able to form due to the wave–outflow interaction between a traveling gravity wave and a cold air outflow. This hypothesis was proved by performing experiments with a steady-state heat sink and an additional transient heat source that is used to generate the traveling gravity waves. With the addition of the transient heating, a density current is able to form for a flow with $U = -9.5$ m s^{-1} (CH2). No density current is able to form in a corresponding case with only one heat sink (C2). The convergence zone associated with the heating induced gravity wave is able to interact nonlinearly with the convergence zone associated with the cold air outflow produced by the prescribed cooling. This nonlinear interaction appears to be responsible for producing the strong upward motion and reversed flow. Once the density current forms, the disturbance becomes highly nonlinear and tends to modify the basic state. For a flow with $U = -11$ m s^{-1} (CH3), the disturbance near the cooling center is suppressed almost completely by the downstream-traveling gravity wave. Unlike the correspond-

ing cooling case (C3), no density current is able to form in 10 h. It appears that the divergence zone associated with the heating-induced gravity wave tends to suppress the convergence zone located just upstream of the cooling center. This process, in turn, weakens the upward motion. It appears that the interaction of gravity waves and outflows is wholly nonlinear and not a simple linear superposition of both disturbances. For a flow with $U = -13$ m s^{-1} (CH4), a density current is able to form at about $t = 5$ h, which does not form in the corresponding cooling case (C4). Thus, the wave–outflow interaction may be constructive or destructive depending upon the characteristics of the flow and the prescribed thermal forcings.

The same idea is then applied to a stably stratified uniform flow over two heat sinks. In a quiescent fluid, a region of cold air, convergence, and upward motion is formed at the center of the coupled heat sinks after the collision between two cold air outflows generated by the coolings. This region of cold air and upward motion then remains at the same location as time proceeds since the continuous coolings have the same strength. After the collision, the cold air outflows lose their own identity and merge into a stationary cold pool. It is also found that the gravity waves tend to suppress this new, stationary cold air outflow after collision. The region of upward motion associated with the collision is confined in a very shallow layer, and it does not seem that new convection can be triggered even if the flow is moist. This result is different from that of Droegemeier and Wilhelmson (1985a,b). In a moving airstream, the response of the flow to two heat sinks is quite dramatic. In the case with $U = -8$ m s^{-1} (CC1), a new density current forms, while the left density current is suppressed significantly and the right density current is suppressed slightly. The suppression or enhancement of the density current is caused by the gravity wave forced by the nearby cooling. In the case with $U = -9.5$ m s^{-1} (CC2), a density current is able to form, although it cannot form in a corresponding case with only one cooling (C2). The mechanism responsible for the formation of this density current is the wave–outflow interaction. The upstream-propagating gravity wave (wave I) produced by the downstream heat sink is able to propagate through the cold air produced by the upstream heat sink. The convergence or upward motion associated with this wave is able to interact with the cold air outflow associated with the upstream heat sink to form the density current.

In order to apply the present theory to the real atmosphere, the theory should be extended to a structured atmosphere that physically represents a better model of the true wave reflection mechanisms of the middle troposphere. In addition, the vertical wind shear and latent heating should also be considered in the model. In such environments, the wave–outflow interaction mechanism may play an important role in triggering new convection in a moist airstream. Due to the time and horizontal scales of cooling used in this study, the results are more applicable for large convective systems rather than individual storms. The present results may not be applicable to a three-dimensional flow passing through an isolated cooling region since the fluid parcels may pass around the heat sink. This implies that the density current will be more difficult to form. However, the present study still provides a meaningful physical insight into the response and fundamental dynamics associated with wave–outflow interactions for a stably stratified flow over thermal forcings. With the boundary-layer physics included, the upward motion ahead of the cold air outflow may be enhanced by the additional convergence. This implies that a density current may be easier to form. However, this still needs to be proved by using a model with the boundary-layer physics included.

Acknowledgments. Discussion with R. Rotunno and comments from Dr. M. W. Moncrieff and two anonymous reviewers are highly appreciated. The authors wish to thank Dr. Neng-Huei Lin for helping to develop the plotting programs and to Mr. Robert A. Rozumalski for helping to draw Fig. 14. This work is partially supported by NASA Grant NAG 5-1790 and NOAA Grant GC91112.

REFERENCES

Asselin, R., 1972: Frequency filter for time integrations. *Mon. Wea. Rev.*, **100,** 487–490.

Bretherton, C., 1988: Group velocity and the linear response of stratified fluids to internal heat or mass sources. *J. Atmos. Sci.*, **45,** 81–93.

Charba, J., 1974: Application of gravity current model to analysis of squall-line gust front. *Mon. Wea. Rev.*, **102,** 140–156.

Chun, H.-Y., 1991: Role of a critical level in a shear flow with diabatic forcing. Ph.D. dissertation, North Carolina State University, 159 pp.

Crook, N. A., and M. W. Moncrieff, 1988: The effect of large-scale convergence on the generation and maintenance of deep moist convection. *J. Atmos. Sci.*, **45,** 3606–3624.

Droegemeier, K. K., and R. B. Wilhelmson, 1985a: Three-dimensional numerical modeling of convection produced by interacting thunderstorm outflows. Part I: Control simulation and low-level moisture variations. *J. Atmos. Sci.*, **42,** 2381–2403.

——, and ——, 1985b: Three-dimensional numerical modeling of convection produced by interacting thunderstorm outflows. Part II: Variations in vertical wind shear. *J. Atmos. Sci.*, **42,** 2404–2414.

Goff, R. C., 1975: Thunderstorm outflow kinematics and dynamics. NOAA Tech. Memo., ERL NSSL-75, 63 pp.

Holle, R. L., and M. W. Maier, 1980: Tornado formation from downdraft interaction in the FACE mesonetwork. *Mon. Wea. Rev.*, **108,** 1010–1028.

Klemp, J. B., and D. K. Lilly, 1978: Numerical simulation of hydrostatic mountain waves. *J. Atmos. Sci.*, **35,** 78–107.

——, and D. R. Durran, 1983: An upper boundary condition permitting internal gravity wave radiation in numerical mesoscale models. *Mon. Wea. Rev.*, **111,** 430–444.

Lin, Y.-L., 1986: Calculation of airflow over an isolated heat source with application to the dynamics of V-shaped clouds. *J. Atmos. Sci.*, **43,** 2736–2751.

——, and R. B. Smith, 1986: Transient dynamics of airflow near a local heat source. *J. Atmos. Sci.*, **43,** 40–49.

——, and H.-Y. Chun, 1991: Effects of diabatic cooling in a shear flow with a critical level. *J. Atmos. Sci.*, **48,** 2476–2491.

Lindzen, R. S., and K.-K. Tung, 1976: Banded convective activity and ducted gravity waves. *Mon. Wea. Rev.*, **104,** 1602–1617.

Ludlam, F. H., 1963: Severe local storms: A review. *Meteor. Monogr.*, No. 5, Amer. Meteor. Soc., 1–30.

Mitchell, K. E., and J. B. Hovermale, 1977: A numerical investigation of a severe thunderstorm gust front. *Mon. Wea. Rev.*, **105,** 657–675.

Mueller, C. K., and R. E. Carbone, 1987: Dynamics of a thunderstorm outflow. *J. Atmos. Sci.*, **44,** 1879–1898.

Newton, C. W., 1966: Circulations in large sheared cumulonimbus. *Tellus,* **18,** 699–713.

Orlanski, I., 1976: A simple boundary condition for unbounded hyperbolic flows. *J. Comput. Phys.*, **21,** 251–269.

Perkey, D. J., 1976: A description and preliminary results from a fine mesh model for forecasting quantitative precipitation. *Mon. Wea. Rev.*, **104,** 1513–1526.

Raymond, D. J., 1986: Prescribed heating of a stratified atmosphere as a model of moist convection. *J. Atmos. Sci.*, **43,** 1101–1111.

——, and R. Rotunno, 1989: Response of a stably stratified flow to cooling. *J. Atmos. Sci.*, **46,** 2830–2837.

Rotunno, R., J. B. Klemp, and M. L. Weisman, 1988: A theory for strong, long-lived squall lines. *J. Atmos. Sci.*, **45,** 463–485.

Schmidt, J. M., and W. R. Cotton, 1990: Interactions between upper and lower tropospheric gravity waves on squall line structure and maintenance. *J. Atmos. Sci.*, **47,** 1205–1222.

Scorer, R. S., 1949: Theory of lee waves of mountains. *Quart. J. Roy. Meteor. Soc.*, **75,** 41–56.

Seitter, K. L., 1986: A numerical study of atmospheric density current motion including the effects of condensation. *J. Atmos. Sci.*, **43,** 3068–3076.

Simpson, J., 1980: Downdrafts as linkages in dynamic cumulus seeding effects. *J. Appl. Meteor.*, **19,** 477–487.

Simpson, J. E., 1982: Gravity currents in the laboratory, atmosphere, and ocean. *Ann. Rev. Fluid Mech.*, **14,** 213–234.

Sinclair, P. C., and J. F. W. Purdom, 1983: The genesis and development of deep convective storms. NOAA/CIRA Report, 56 pp.

Smith, R. B., and Y.-L. Lin, 1982: The addition of heat to a stratified airstream with application to the dynamics of orgraphic rain. *Quart. J. Roy. Meteor. Soc.*, **108,** 353–378.

Tao, W.-K., and J. Simpson, 1984: Cloud interactions and merging: Numerical simulations. *J. Atmos. Sci.*, **41,** 2901–2917.

Thorpe, A. J., M. J. Miller, and M. W. Moncrieff, 1980: Dynamical models of two-dimensional downdraughts. *Quart. J. Roy. Meteor. Soc.*, **106,** 463–484.

——, ——, and ——, 1982: Two-dimensional convection in non-constant shear: A model of mid-latitude squall lines. *Quart. J. Roy. Meteor. Soc.*, **108,** 739–762.

Westcott, N., 1984: A historical perspective on cloud mergers. *Bull. Amer. Meteor. Soc.*, **65,** 219–226.

Zipser, E. J., 1969: The role of unsaturated convective downdrafts in the structure and rapid decay of an equatorial disturbance. *J. Appl. Meteor.*, **8,** 799–814.